AGU PUBLICATIONS

Tectonics

RESEARCH ARTICLE
10.1002/2015TC003895

Key Points:
- Stress inversion provides a transpressional first-order stress field
- The plate boundary is characterized by more distribution of tectonic regime
- The current surface deformation may influenced by mantle-lithosphere interaction

Correspondence to:
A. Soumaya,
abdelkader.soumaya@onm.nat.tn

Citation:
Soumaya, A., N. Ben Ayed, D. Delvaux, and M. Ghanmi (2015), Spatial variation of present-day stress field and tectonic regime in Tunisia and surroundings from formal inversion of focal mechanisms: Geodynamic implications for central Mediterranean, *Tectonics*, *34*, 1154–1180, doi:10.1002/2015TC003895.

Received 27 MAR 2015
Accepted 6 MAY 2015
Accepted article online 10 MAY 2015
Published online 16 JUN 2015

Spatial variation of present-day stress field and tectonic regime in Tunisia and surroundings from formal inversion of focal mechanisms: Geodynamic implications for central Mediterranean

Abdelkader Soumaya[1,2], Noureddine Ben Ayed[3], Damien Delvaux[4], and Mohamed Ghanmi[2]

[1]Service Géologique, Office National des Mines, Tunis, Tunisia, [2]Département de Géologie, FST, Université Tunis El Manar, Tunis, Tunisia, [3]Faculté des Sciences de Bizerte, Bizerte, Tunisia, [4]Earth Sciences Department, Royal Museum for Central Africa, Tervuren, Belgium

Abstract We compiled 123 focal mechanisms from various sources for Tunisia and adjacent regions up to Sicily, to image the current stress field in the Maghrebides chain (from Tunisia to Sicily) and its foreland. Stress inversion of all the available data provides a first-order stress field with a N150°E horizontal compression (S_{Hmax}) and a transpressional tectonic regime, but the obtained stress tensor poorly fit to the data set. We separated them into regional subsets (boxes) in function of their geographical proximity, kinematic regime, homogeneity of kinematic orientations, and tectonic setting. Their respective inversion evidences second- and third-order spatial variations in tectonic regime and horizontal stress directions. The stress field gradually changes from compression in the Maghrebides thrust belt to transpression and strike slip in the Atlassic and Pelagian foreland, respectively, where preexisting NW-SE to E-W deep faults system are reactivated. This spatial variation of the sismotectonic stress field and tectonic regime is consistent with the neotectonic stress field determined by others from fault slip data. The major Slab Transfer Edge Propagator faults (i.e., North-South Axis-Hammamet relay and Malte Escarpment), which laterally delimit the subducting slabs, play an active role in second- and third-order lateral variations of the tectonic regime and stress field orientations over the Tunisian/Sicilian domain. The past and current tectonic deformations and kinematics of the central Mediterranean are subordinately guided by the plate convergence (i.e., Africa-Eurasia), controlled or influenced by lateral slab migration/segmentation and by deep dynamics such as lithosphere-mantle interaction.

1. Introduction

The Africa-Eurasia plate boundary is largely represented by an orogenic belt running from Morocco to Sicily [e.g., *McClusky et al*., 2003; *Nocquet and Calais*, 2004; *Serpelloni et al*., 2007]. It is characterized by deep basins and curved fault-and-thrust belts derived from the long-lasting plate convergence between Nubia/Eurasia since the Late Cretaceous [e.g., *Le Pichon et al*., 1988]. At the scale of lithospheric plates, Africa moves with respect to Eurasia in a NW direction at a rate of ~0.5 cm/yr [*Nocquet*, 2012]. This convergence is accommodated mainly in the Maghrebides belt in western-central Mediterranean [*Serpelloni et al*., 2007], which is partitioned between two almost parallel E-W trending belts From Morocco to Sicily. In central Mediterranean, the Africa-Europe convergence is mainly accommodated in the southern Tyrrhenian area [*Nocquet*, 2012].

Since the initiation of the World Stress Map project (WSM) in 1986, several studies have been undertaken to characterize the current stress field [*Zoback*, 1992]. In the case of the central Mediterranean region, neotectonic and seismotectonic studies were performed to determine the stress pattern acting on the European side of the Europe-Africa plate boundary [e.g., *Bousquet and Philip*, 1981; *Philip*, 1987; *Rebaï et al*., 1992; *Montone et al*., 2004; *Heidbach et al*., 2010] and on the African side in North Africa [e.g., *Rebaï et al*., 1992; *Buforn et al*., 2004; *Serpelloni et al*., 2007; *Meghraoui and Pondrelli*, 2012]. They revealed a general trend in the orientation of the maximum horizontal stress (S_{Hmax}) which is directed NW-SE to N-S with local deviations related to the large geological structures. Over the Tunisian territory, the data of current stress state are relatively scarce and poorly documented in the literature [*Ben Ayed and Zargouni*, 1990; *Chihi*, 1992; *Bahrouni et al*., 2014].

Recently, there has been a significant increase in the number of earthquake focal mechanisms available for Tunisia and its surroundings, due to the upgrade of the seismic network, a longer observation period, and the improvement of numerical methods for focal mechanism determination. Within mainland Sicily and adjacent offshore areas, several studies documented that the seismotectonic deformations are of compressional type with a strike-slip component and NW-SE to N-S oriented horizontal *p* kinematic axis for the majority of the focal mechanisms [e.g., *Montone et al*., 2004; *Pondrelli et al*., 2006; *Lavecchia et al*., 2007; *Catalano et al*., 2008; *Macchiavelli et al*., 2012]. The eastern Sicily Island and its northern side represent one of the most seismically active regions of central Mediterranean [*Catalano et al*., 2009]. Seismotectonic analysis and in stress situ measurements [*Ragg et al*., 1999] demonstrate the occurrence of a still active compressional regime around the Mount Etna region [*Catalano et al*., 2009].

This work intends to provide a new picture of the current stress state, tectonic regime, and their variation in different structural domains of Tunisia and neighboring areas. We compiled 123 focal mechanisms from different catalogues, distributed throughout the study area. We use the Frohlich triangle [*Frohlich*, 1992] to classify the kind of focal mechanisms and a formal tectonic stress inversion with the Win-Tensor program [*Delvaux et al*., 1997; *Delvaux and Sperner*, 2003; *Delvaux and Barth*, 2010] to determine the tectonic stress field. The lateral variations of the current stress field are determined at the scale of second- and third-order stress pattern as defined by *Heidbach et al*. [2010].

2. Geodynamic Framework

Over the entire Mediterranean region, the subduction process is underlined by an increasing of slab rollback under the combined action of decreasing velocity of the African plate and increasing slab pull force [e.g., *Wortel and Spakman*, 2000; *Jolivet and Faccenna*, 2000; *Faccenna et al*., 2004; *Billi et al*., 2011]. During plate convergence in the central Mediterranean segment, *Faccenna et al*. [2004, 2005] envisaged three episodes of slab break-off (10–8 Ma, 5–4 Ma, and 1–0.8 Ma) on the basis of the timing of changes of magmatism, tomographic data, and the estimation of trench retreat along the subducting plate boundary. In particular, magmatism changes from calc-alkaline (14–10 Ma) in the Galite Island and Nefza (northern Tunisia) to alkaline basalts (10–8 Ma) in Mogodos, Wadi Bellif, and Guelb Saad Moun [*Maury et al*., 2000]. This change is interpreted as resulting from a lateral separation of the Calabrian slab [*Faccenna et al*., 2005] from the inactive northern African (Tell) slab [*Casero and Roure*, 1994]. As a consequence, the mantle return flows around the broken slab which became free to retreat eastward within the Tyrrhenian domain [*Faccenna et al*., 2004; *Billi et al*., 2011]. Heat input from this uprising asthenosphere may have warmed up the continental crust and facilitated its assimilation by the mantle. This caused a regional metamorphism, hydrothermalism (e.g., in Ichkeul and Hairech massif, north Tunisia), and mineralization, in response to tearing and detachment of the slab since the Late Tortonian-Pliocene.

Rupture of the slab also favored the rapid onset of continental collision in Late Tortonian and was associated to uplift, thrusting at the basal contact of the Tellain nappes [*Rouvier*, 1977], and edification of the Maghrebides thrust belt along the Tunisian-Sicily coast [*Argnani*, 2009]. This event propagated to the central Tunisian foreland and was followed by molassic deposition in subsiding fore-deep basins during the Pliocene. During the second slab break-off within the Sicily Channel (5–4 Ma), an intense back-arc extension occurred in the South Tyrrhenian Sea, enlargement of slab windows and thrusting ended in the Adventure Maghrebides thrust belt [e.g., *Argnani*, 2009], as the tear migrated eastward [*Faccenna et al*., 2004]. The Sicily Strait, which opened contemporaneously with the Tyrrhenian basin by slab pull-related rifting, could be the surface manifestation of this second slab break-off [*Faccenna et al*., 2004]. This rift system in the Sicily Channel, developed in the African foreland area and cutting the inactive thrust system, is characterized by Quaternary magmatic activity [*Argnani*, 2009]. During the late Pliocene-Quaternary (4–2 Ma), the ENE trending molassic basins of northern Tunisia and the southern back-arc Tyrrhenian margin were inverted into a compressive regime, still active today. At this time, the backward migration of the slab was favored by the separation of the oceanic Ionian area from the contiguous floatable continental domains [*Faccenna et al*., 2005].

Based on geological and geochemical data and tomographic images, *Faccenna et al*. [2005] demonstrated that the locking of the subduction trench is due to the formation and enlargement of slab window along

the Sicilian Maghrebides. At Calabrian arc, where its outward migration is not hampered by continental collision [*De Voogd et al*., 1992], the presence of intermediate to deep seismicity and strong uplift are interpreted as evidence of slab detachment beneath this arc since 700 ka [*Wortlel and Spakman*, 2000]. As a result, the subducting central Mediterranean lithosphere was progressively fragmented, forming isolated, narrow, and fast retreating slabs beneath and near the Maghrebides collisional belt [e.g., *Faccenna et al*., 2004; *Guillaume et al*., 2013]. This subduction process occurs along a significant portion of the current plate boundary. This raises several questions relative to the neotectonic evolution of the eastern Maghrebian margin (central Mediterranean) and on the role of inherited structures on the sismotectonic reactivation process.

3. Data Compilation and Box Zonation

We compiled the available single-event focal mechanism data for Tunisia and its surroundings from the Harvard Global Centroid Moment Tensor (CMT), the Euro-Mediterranean Regional Catalog (RCMT), the Istituto Nazionale Geofisica e Vulcanologia (INGV) [*Pondrelli et al*., 2006], and the ETH Zurich (ETHZ) [*Braunmiller et al*., 2002] catalogs, completed by additional published mechanisms [e.g., *Bernardi et al*., 2004]. We collected 118 individual focal mechanisms for 1957 to 2014 (Figures 1 and 2 and Table 1). Focal mechanisms are listed in Table 1 with their strike-, dip-, and rake-derived horizontal principal stress directions (S_{Hmax} and S_{Hmin}) according to *Lund and Townend* [2007] and their type according to the WSM Project standard (NF: normal faulting, SS: strike slip, TF: thrust faulting, NS: oblique-normal, TS: oblique-reverse, and U: unknown type).

These focal mechanisms are located mainly in seismically active areas in northern Tunisia, in Saharan Atlas, Pelagian Plateau, and Sicily area. They correspond to seismic events with M_w ranging from 2 to 6. The spatial distribution of focal mechanisms shows that the orientation of the S_{Hmax} and S_{hmin} axes and the focal mechanism type are relatively homogeneous in Tunisia and surrounding areas, with however lateral variations (Figures 2 and 3).

According to *Heidbach et al*. [2010], the intraplate tectonic stress field can be defined as a function of the spatial scale of study: the first-order stress field driven by plate boundary is primarily oriented in parallelism with the absolute plate motion; second-order stress field is caused by lithospheric flexure and intraplate lateral density contrasts such as those associated with continental rifting, isostatic compensation, topography, and deglaciation; and the third-order stress field corresponds to the local stress source at the scale of less than 100 km, influenced by the structural geometry, interaction between fault systems, topography, or local density contrasts. The first-order stress field will be illustrated by the stress inversion of the entire database, while in order to image the second- and third-order stress fields, we subdivided the study area into five boxes and inverted each box separately (Figure 2).

The boxes are defined as corresponding to known structural domains, in which the focal mechanisms are of relatively similar type and deformation is relatively homogeneous. They cover the most actively deforming parts of the study area. We used boxes which are sufficiently wide and contain a sufficiently large number of focal mechanisms as they reflect both the stress regime and the orientation of the preexisting faults. Therefore, different structural domains may be presently undergoing the same stress regime but displaying variations in their focal mechanisms. Defining too small boxes might produce a false impression of stress field variation because it might also reflect the heterogeneity of the reactivated structures. Large boxes allow also avoiding a priori definition of stress provinces, preserving room for further spatial separation of the data during the stress inversion process.

4. Classification of Focal Mechanisms Using the Frohlich Diagram

The Frohlich triangle diagram is a graphical method for displaying focal mechanisms as a function of dip angle relative to the horizontal of *P*, *T*, and *B* axes [*Frohlich*, 1992] (Figures 3, 4a, and 4b). It allows defining the type of focal mechanism and provides a way for quantifying the relative proportion of normal, thrust, and strike-slip focal mechanisms. They are classified as normal faulting (NF) when the *P* axis is subvertical (>60°), thrust faulting (TF) when the *T* axis is subvertical (>50°), strike slip (SS) when the *B* axis is subvertical (>60°), and "odd" mechanisms for the others. The data are plotted for each box on the Frohlich

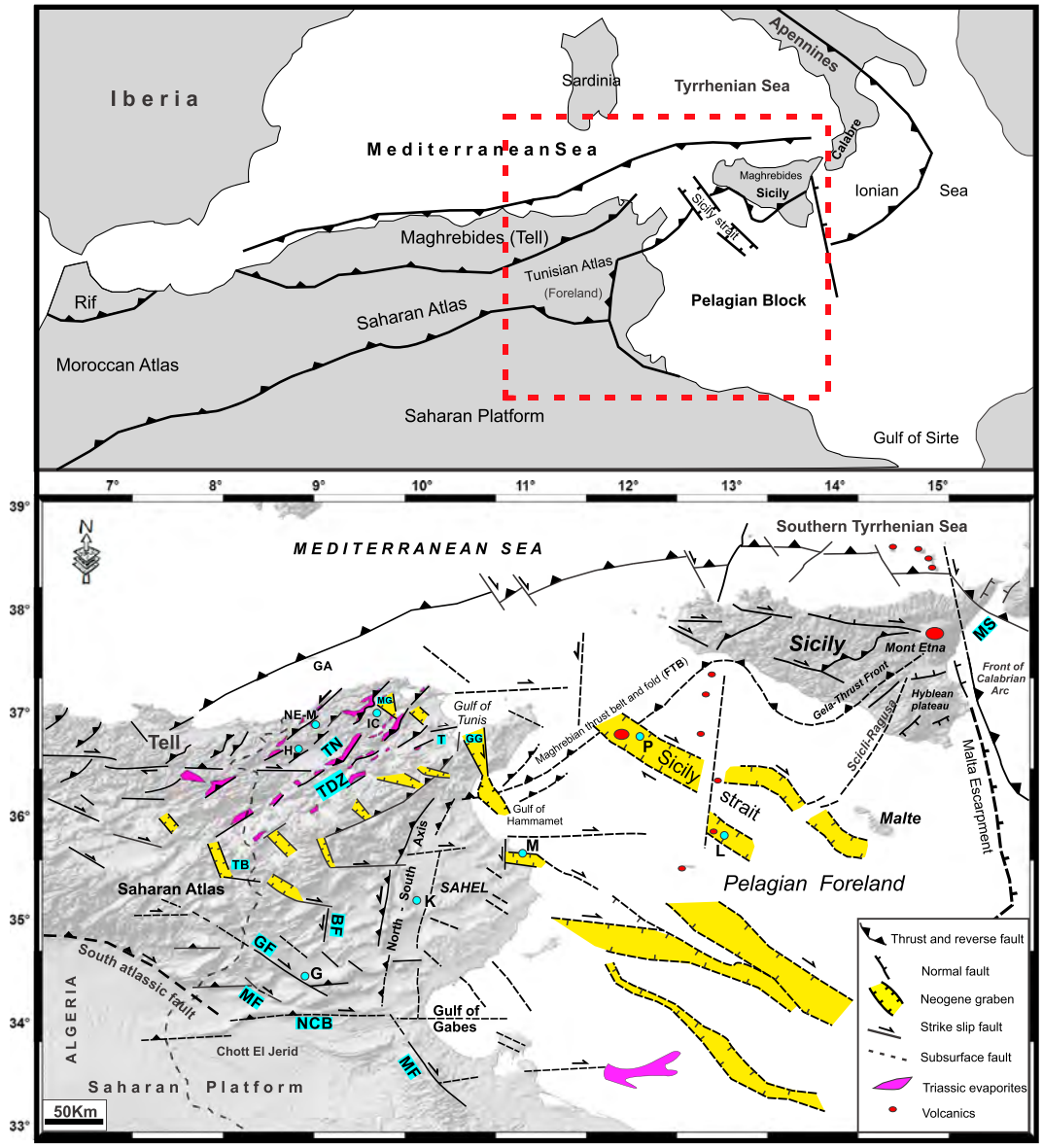

Figure 1. Tectonic sketch of Tunisia and surrounding regions with location of the study area. TN: Tellain nappes (Maghrebides), TDZ: Triassic diapirs zone, MG: Mateur graben, GA: Galite Island, NE-M: Nefza-Mogodos, Hairech, Ichkeul, GG: Grombalia graben, K: Kairouan, MF: Metlaoui fault, BF: Bir Hfey fault, GF: Gafsa fault, G: Gafsa region, T: Tunis, TB: Tebessa, M: Monastir region, P: Pantelleria Island, L: Linosa, NCB: northern Chott fault, MF: Medenine fault system, and MS: Messinian Strait.

ternary diagram using color coding according to the focal mechanism type: red for normal faulting, green for strike slip, blue for thrust faulting, and composite colors for mixed type (Figure 4).

The triangular plots for northern Tunisia (box 1) show the predominance of TF and SS focal mechanisms with some normal mechanisms indicating local extensions. The plots for the North-South Axis (box 2) show a dominance of thrust (TF) and a few strike-slip (SS) focal mechanisms with subhorizontal *P* axis (Figure 4). The Saharan Atlas zone and the Pelagian platform (boxes 3 and 4) are both dominated by strike-slip (SS) focal mechanisms, all with a subvertical *B* axis. They have relatively steep *T* axes for the Atlassic zone, indicating a thrust-faulting component, and weakly inclined *P* axes for the Pelagian domain, indicating a normal faulting component (Figure 4).

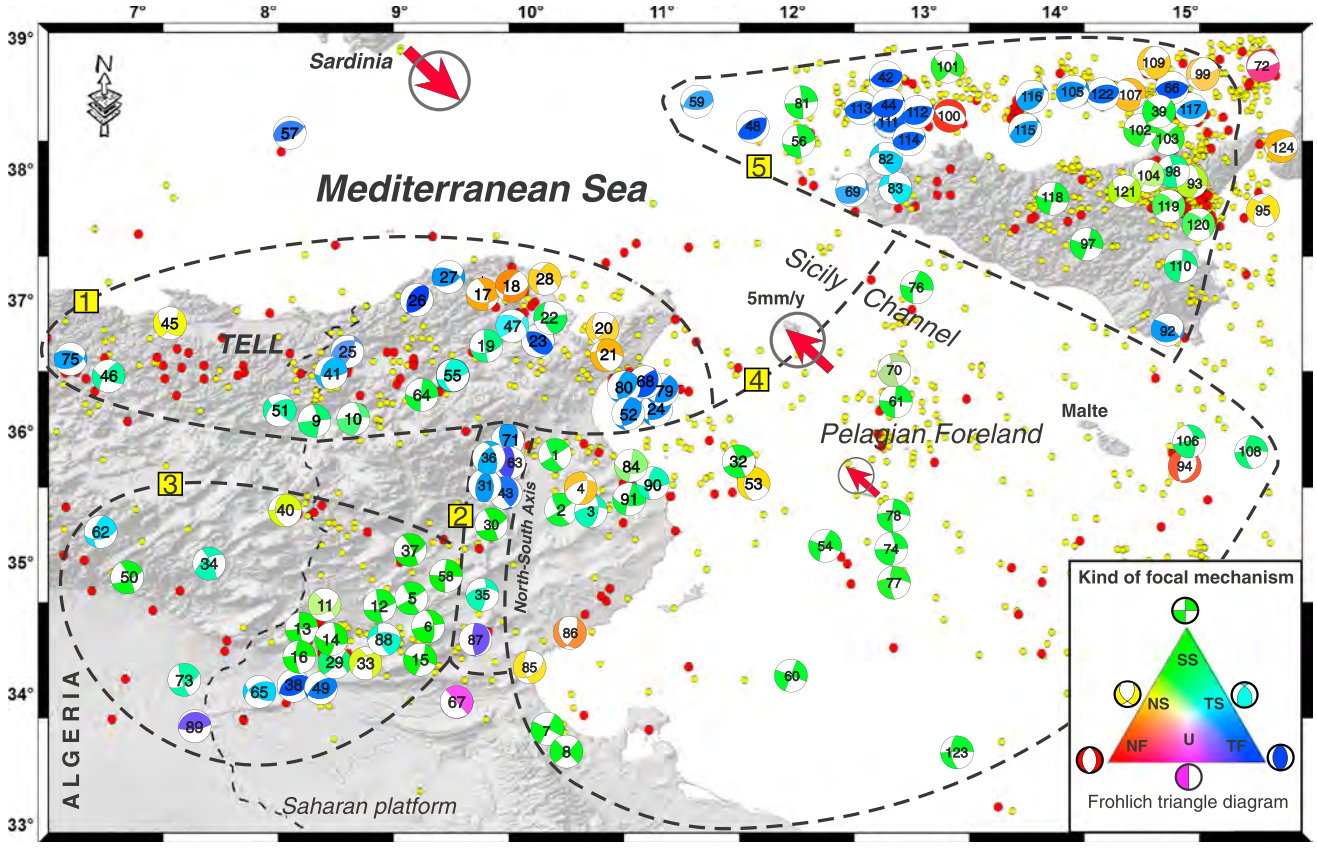

Figure 2. Grouping of focal mechanism data into boxes for stress inversion. Boxes: 1–northern Tunisia, 2–North-South Axis, 3–Saharan Atlas, 4–Pelagian foreland, and 5–Sicily zone. Seismicity data (National Institute of Meterology for Tunisia and INGV catalog for Sicily and its surroundings): red circle ($M_w \geq 4$) and yellow circle ($3 \leq M_w < 4$). The color of focal mechanisms type is based on the Frohlich triangle diagram (below right): NF: normal faulting, TF: thrust faulting, SS: strike-slip faulting, TS: thrust to strike-slip type, and NS: normal to strike-slip type. Red arrows: velocity field in a Eurasia/Nubia fixed reference frame [*Nocquet*, 2012] and purple arrows: the motion vectors of points south of the seismically active belts in northern Africa [*Serpelloni et al.*, 2007].

5. Tectonic Stress Inversion of the Focal Mechanisms

In the World Stress Map [*Zoback*, 1992; *Heidbach et al.*, 2010], the large majority of stress indicators are earthquake focal mechanisms, and the stress field is determined according to the type of focal mechanism (normal, strike slip, and thrust faulting) and the orientation of the greatest least inclined stress axes, taken as representative for the horizontal principal compression (S_{Hmax}). This is assuming that there is a statistical correspondence between the *P*, *B*, and *T* kinematic axes of the focal mechanisms and the stress axes σ_1, σ_2, and σ_3. However, the kinematic axes are related geometrically to the orientation of the fault plane activated during the earthquake. In consequence, the deduced S_{Hmax} orientations depend partly on the orientation of the reactivated plane and therefore on the existing structural pattern. In order to access the four parameters of the reduced tectonic stress tensor, a formal stress inversion is needed. Such methods have been developed in parallel for inverting earthquake focal mechanisms [e.g., *Carey-Gailhardis and Mercier*, 1987; *Gephart*, 1990; *Delvaux and Sperner*, 2003; *Delvaux and Barth*, 2010] and geological fault slip data [e.g., *Carey and Brunier*, 1974; *Angelier and Mechler*, 1977; *Michael*, 1987; *Angelier*, 2002; *Delvaux and Sperner*, 2003].

Here we used the Win-Tensor program [*Delvaux et al.*, 1997; *Delvaux and Sperner*, 2003] according to the procedure used in *Delvaux and Barth* [2010] for the inversion of focal mechanisms.

5.1. Stress Inversion Methodology

Stress inversion methods are based on the assumptions of *Bott* [1959] that the stress field is invariant and homogeneous in space and time in the study region and slip on a fault plane occurs in the direction of

Table 1. Compiled Database of Focal Mechanisms Used in This Study, Grouped in Five Boxes[a]

Date-Time Group		Location			Data				SH		Stress	
No.	Event	Lat	Long	Depth	M_w	Strike	Dip	Rake	Max	Min	Type	Source
						Northern Tunisian (box 1)						
25	19770119	36.50	08.60	10	4.6	253	35	134	138	048	TF	*Hfaiedh et al.* [1985]
28	19790409	37.20	10.10	12	5.0	305	67	−140	161	71	NS	*Hfaiedh et al.* [1985]
41	19770119	36.50	08.60	10	4.6	200	40	030	143	053	TS	*Gueddiche et al.* [1992]
26	19900622	37.09	09.35	10	2.8	043	45	101	125	035	TF	*Gueddiche et al.* [1992]
27	19900718	37.12	09.40	8.6	2.0	063	51	050	001	091	TF	*Gueddiche et al.* [1992]
47	19701201	36.90	09.95	15	5.1	049	74	050	175	085	TS	*Gueddiche et al.* [1992]
64	19570220	36.40	09.00	-	5.2	185	87	018	139	049	SS	*Vannucci and Gasperini* [2004]
10	19981203	36.04	08.46	18	3.4	002	53	010	134	044	SS	*Bahrouni et al.* [2014]
09	20010506	36.16	08.34	8	3.4	353	72	001	128	038	SS	*Bahrouni et al.* [2014]
51	19970305	36.20	08.21	14	3.2	234	49	014	005	095	SS	*Bahrouni et al.* [2014]
17	19930219	37.13	09.57	11	3.9	095	46	−149	128	038	NS	*Mejri* [2012]
19	20010114	36.90	09.63	11	3.1	174	82	035	124	034	SS	*Mejri* [2012]
18	19950126	37.09	09.72	10	4.3	087	42	−039	057	147	NF	*Mejri* [2012]
22	20010608	36.86	10.19	09	3.3	165	60	175	032	122	SS	*Mejri* [2012]
23	20011026	36.70	10.00	10	3.3	295	50	070	040	130	TF	*Mejri* [2012]
20	20010906	36.72	10.56	09	3.5	045	70	−050	011	101	NS	*Mejri* [2012]
21	20010525	36.73	11.09	10	3.2	165	40	−028	133	043	NS	*Mejri* [2012]
55	19940917	36.46	09.17	10	5.6	181	47	020	138	048	TS	RCMT
80	20050207	36.22	10.87	10	4.7	051	41	124	120	030	TF	RCMT
68	20050207	36.22	10.87	6	4.9	222	66	098	122	032	TF	ETHZ
79	20050207	36.09	10.90	09	4.7	207	71	070	141	051	TF	ETHZ
24	20050207	36.10	10.91	10	4.8	067	44	128	133	043	TF	RCMT
52	20050207	36.11	10.83	12	5,1	051	41	124	121	031	TF	RCMT
45	20030920	36.79	07.24	10	6.4	137	50	−159	175	085	NS	RCMT
75	20080602	36.45	06.53	10	4.1	065	48	058	176	086	TF	RCMT
46	19851027	36.43	06.75	10	5.8	213	71	020	165	075	SS	Harvard CMT
						North-South Axis (box 2)						
71	20020624	36.03	10.29	15	5.2	028	48	128	093	003	TF	Harvard CMT
31	20020624	35.85	09.88	9	4.9	352	47	070	096	006	TF	ETHZ
36	20010812	35.90	09.84	6	4.6	340	54	046	100	010	TF	ETHZ
63	20020624	35.85	09.89	10	4.9	174	29	083	088	178	TF	RCMT
43	20010812	35.92	09.81	15	4.6	010	25	122	083	173	TF	RCMT
87	19950922	34.28	09.58	10	3.7	178	75	083	101	011	TF	INMT
30	20010812	35.52	09.92	30	4.3	067	72	−177	111	021	SS	*Mejri* [2012]
35	19791208	34.70	09.74	33	5.4	007	72	035	136	046	SS	*Ben Ayed and Zargouni* [1990]
						Saharan Atlas (box 3)						
12	19960329	34.49	09.32	10	4.4	168	86	014	123	033	SS	*Bahrouni et al.* [2014]
05	19970705	34.40	09.43	13	2.8	150	88	002	105	015	SS	*Bahrouni et al.* [2014]
06	19920313	34.27	09.39	22	4.4	350	61	001	125	035	SS	*Bahrouni et al.* [2014]
13	19900302	34.40	08.50	5	4.4	083	89	170	128	038	SS	*Bahrouni et al.* [2014]
15	19980109	34.13	09.15	15	3.6	289	89	179	154	064	SS	*Bahrouni et al.* [2014]
16	19940511	34.13	08.27	5	4.6	178	72	−003	133	043	SS	*Bahrouni et al.* [2014]
11	19980310	34.46	08.59	18	3.6	056	53	010	008	098	SS	*Bahrouni et al.* [2014]
33	19780208	34.30	09.10	23	4.7	336	68	−148	015	105	SS	*Hfaiedh et al.* [1985]
88	19780208	34.27	09.15	30	5.0	266	54	026	033	123	TS	*Mezcua and Martınez Solares* [1983]
65	19920612	34.20	08.33	19	5,2	242	48	043	000	090	TF	*Vannucci and Gasperini* [2004]
14	19891107	34.33	08.40	12	4.4	104	70	−160	145	055	SS	*Bahrouni et al.* [2014]
34	20011213	35.08	07.47	9	4.6	333	81	027	128	038	TF	ETHZ
37	20011213	35.08	09.00		4.1	332	81	−026	109	019	SS	ETHZ
40	19950922	35.54	07.87	15	5.3	173	41	−008	131	041	NF	RCMT
50	20070709	34.09	07.04	21	4.7	067	77	−170	111	021	SS	RCMT
62	20020131	35.31	06.36	33	4.1	078	54	140	136	046	TS	RCMT
29	20080924	34.20	08.46	27	4.3	309	76	168	175	085	SS	RCMT
58	20101113	35.08	09.42	10	4.0	183	83	000	138	048	SS	RCMT
38	19970320	34.09	08.37	10	5.0	066	44	095	152	062	TF	RCMT
89	20130404	33.75	7.78	10	5.2	256	16	83	169	79	TF	RCMT
73	20070709	34.10	6.89	22	4.8	064	62	165	112	022	SS	Harvard CMT
49	19920612	34.21	08.44	15	5.2	082	36	114	158	068	TF	Harvard CMT

Table 1. (continued)

Date-Time Group		Location			Data				SH		Stress	
No.	Event	Lat	Long	Depth	M_w	Strike	Dip	Rake	Max	Min	Type	Source
						Pelagian Block (box 4)						
77	20061123	35.97	12.94	9	4.6	177	73	−020	135	045	SS	RCMT
78	20111218	36.10	12.90	12	4.7	273	78	−174	138	048	SS	RCMT
53	19890106	35.59	11.69	11	5.2	183	41	−026	148	058	NS	RCMT
74	20061123	35.97	12.94	10	4.8	357	70	−002	132	042	SS	RCMT
70	20090319	36.52	12.72	20	4.4	255	48	−180	119	029	NS	RCMT
54	19930910	35.00	12.40	10	4.4	200	78	001	155	056	SS	Harvard CMT
32	19890103	35.79	11.80	10	5.0	247	89	180	112	022	SS	Harvard CMT
84	20131018	35.70	10.83	12	4.8	099	51	−179	143	053	UF	Harvard CMT
90	20131018	35.61	10.98	10	4.8	101	58	175	147	57	SS	RCMT
91	20131021	35.60	10.93	10	4.6	89	71	156	138	48	SS	RCMT
61	20111218	36.10	12.68	12	4.7	183	85	002	138	048	SS	RCMT
76	20070410	36.96	12.84	28	4.1	100	84	164	147	057	SS	RCMT
85	20020624	34.30	10.27	-	3.5	056	50	−037	024	114	NS	INMT
86	20070709	34.47	10.35	-	3.5	024	64	−063	003	093	NF	INMT
94	20110424	35.80	14.90	19	4.20	28	34	−76	20	110	NF	INGV
01	19970403	36.05	10.13	7	3.8	149	75	002	103	013	SS	*Bahrouni et al.* [2014]
02	19950130	35.51	10.20	6	4.5	166	90	−143	031	121	UF	*Bahrouni et al.* [2014]
03	19950204	35.52	10.29	6	4.0	264	69	141	137	047	TS	*Bahrouni et al.* [2014]
04	19950201	35.53	10.32	4	4,1	009	55	−137	040	130	NF	*Bahrouni et al.* [2014]
07	20010509	33.54	10.30	14	4.0	027	89	002	162	072	SS	*Bahrouni et al.* [2014]
08	19980105	33.51	10.11	16	4.7	046	83	001	001	091	SS	*Bahrouni et al.* [2014]
106	20030707	35.85	14.97	15	-	350	62	4	124	34	SS	*Pondrelli et al.* [2006]
108	20061124	35.70	15.50	22	4.40	176	77	8	130	40	SS	*Pondrelli et al.* [2006]
123	19880326	33.41	13.29	15	5.1	176	61	−5	132	42	SS	Harvard CMT
60	19901111	33.94	12.03	10	4.7	291	90	−180	156	066	SS	Harvard CMT
						Sicily zone (box 5)						
81	19950531	37.91	12.28	6	3.9	355	85	−003	130	040	SS	*Vannucci and Gasperini* [2004]
48	19991230	38.32	11.89	10	4,9	050	33	082	145	055	TF	RCMT
56	19950529	37.90	12.07	11	2,8	082	70	−180	127	037	SS	RCMT
69	19810607	37.67	12.47	18	4.9	048	29	048	162	072	TF	RCMT
59	19791208	38.28	11.74	33	5.4	235	45	067	160	070	TF	RCMT
42	19980621	38.43	12.67	10	4.4	088	38	102	171	081	TF	RCMT
44	19980117	38.40	12.90	15	4.4	058	29	071	159	069	TF	RCMT
66	20141009	38.50	14.70	13	4.1	87	35	91	176	86	TF	INGV
39	20140114	38.40	14.80	15	4.2	46	75	7	0	90	SS	INGV
92	20131215	36.70	14.90	10	4.10	75	24	37	013	103	TF	INGV
93	20110506	37.80	15.00	23	4.30	02	50	−17	143	053	SS	INGV
97	20081128	37.40	14.30	32	4.30	17	84	−2	152	62	SS	INGV
98	20121122	37.80	14.90	30	4.10	253	60	173	120	030	SS	INGV
99	20120704	38.60	15.10	182	4.30	177	26	−162	034	124	UF	INGV
100	20120413	38.30	13.30	14	4.40	281	39	−102	108	018	NF	INGV
101	20120225	38.70	13.40	50	4.40	31	69	−18	169	79	SS	INGV
102	20111115	38.30	14.60	14	4.20	06	60	−7	143	53	SS	INGV
103	20100813	38.30	14.80	12	4.70	313	73	−163	175	085	SS	INGV
104	20091219	37.80	14.90	19	4.30	119	47	−178	164	074	UF	INGV
105	20090907	38.50	14.20	17	4.80	276	41	124	165	075	TF	INGV
110	19901213	37.25	14.90	15	5.6	274	64	174	141	51	SS	Harvard CMT
107	19920425	38.56	14.67	247	5.1	332	42	−43	124	034	NF	Harvard CMT
121	19780415	37.77	14.63	33	6	135	60	−176	179	089	SS	Harvard CMT
122	19800528	38.48	14.25	19	5.7	83	43	99	157	077	TF	Harvard CMT
109	20040505	38.60	14.70	253	5.50	178	35	−151	031	021	UF	*Pondrelli et al.* [2006]
111	19980621	38.36	12.70	10	4.60	88	38	102	171	081	TF	*Pondrelli et al.* [2006]
112	19980117	38.40	12.90	10	4.90	260	62	100	159	069	TF	*Pondrelli et al.* [2006]
113	19980620	38.46	12.71	10	5.20	69	22	76	167	077	TF	*Pondrelli et al.* [2006]
114	19980621	38.12	12.85	12	4.60	69	38	77	167	077	TF	*Pondrelli et al.* [2006]
115	20020927	38.31	13.73	15	5.1	41	39	70	143	053	TF	*Pondrelli et al.* [2006]
116	20020906	38.44	13.78	15	5.9	37	42	64	143	053	TF	*Pondrelli et al.* [2006]
117	20020405	38.44	15.01	15	4.4	90	41	108	169	079	TF	*Pondrelli et al.* [2006]
118	20051121	37.70	14.08	45	-	102	79	179	146	056	SS	*Pondrelli et al.* [2006]

Table 1. (continued)

Date-Time Group		Location			Data				SH		Stress	
No.	Event	Lat	Long	Depth	M_w	Strike	Dip	Rake	Max	Min	Type	Source
119	20021027	37.70	14.90	10	4.9	320	60	171	008	098	SS	*Pondrelli et al.* [2006]
120	20021029	37.65	15.07	10	4.7	316	61	−173	000	090	SS	*Pondrelli et al.* [2006]
82	19680115	37.75	12.98	10	5.5	270	50	035	033	123	TS	*Vannucci and Gasperini* [2004]
83	19680125	37.68	12.96	03	5.2	270	64	031	037	127	TS	*Vannucci and Gasperini* [2004]
					Others (not used in the stress inversion)							
57	19770828	38.21	08.21	10	5.0	258	29	104	160	070	TF	RCMT
67	20050207	33.80	09.50	10	5.2	075	02	−153	107	017	UF	ETHZ
95	20021029	37.56	15.69	10	4.2	207	54	−28	171	81	NS	RCMT
72	20061026	38.67	15.40	216	5.0	250	10	−97	74	164	UF	RCMT
124	20120828	38.20	15.80	51	4.8	104	40	−52	80	170	NF	RCMT

[a]Date-time group: followed by date (day-month-year); location: long—longitude (east), lat—latitude, and depth (km); focal mechanism data: M_w—moment magnitude, strike, dip, and rake of focal plane; horizontal stress orientations SH: max—S_{Hmax} and min—S_{Hmin}; source—origin of data: INMT: National institute of Meterology (Tunisia); RCMT: European Mediterranean Regional Centroid Moment Tensor (RCMT) catalog, www.bo.ingv.it/RCMT; and ETHZ: Swiss Seismological catalog, www.seismo.ethz.

maximum resolved shear stress. Most of the inversion methods rely on the observation that resolved normal and shear stress magnitudes and shear stress direction on a plane depend only on four parameters out of six of the complete stress tensor: the principal stress axes σ_1, σ_2, and σ_3 with $\sigma_1 \geq \sigma_2 \geq \sigma_3 \geq 0$ and the ratio of principal stresses $R = (\sigma_2 - \sigma_3)/\sigma_1 - \sigma_3)$ with $0 \leq R \leq 1$. Therefore, fault slip and focal mechanism data constrain only these four parameters which form the reduced stress tensor [*Gephart and Forsyth*, 1984; *Angelier*, 2002].

With focal mechanisms, an additional uncertainty is introduced as it is composed of two nodal planes, one representing the actual fault plane and the other, the auxiliary or virtual plane. A series of computer programs have been developed to consider this ambiguity [e.g., *Carey-Gailhardis and Mercier*, 1987; *Reches et al*., 1992; *Angelier*, 2002; *Delvaux and Sperner*, 2003].

Within the Win-Tensor program [*Delvaux and Sperner*, 2003], the data are first processed using the improved "Right Dihedron method," initially developed by *Angelier and Mechler* [1977]. It provides an initial and approximate stress tensor that is used as a starting point in the "Rotational Optimization" method, which is an iterative method that minimizes a misfit function for each earthquake *c* (F3 in *Delvaux and Sperner* [2003] and F5 in Win-Tensor). The misfit function used comprises two components. The first uses the misfit angle α between the earthquakes slip *b* direction and the computed resolved shear stress of the applied stress tensor on fault planes. The second component uses the nondirectional component of the resolved stress on the fault planes for promoting slip on the fault plane, maximizing the shear stress magnitude $|\tau(c)|$ in order to favor slip and minimizing the normal stress magnitude $|\nu(c)|$ in order to reduce the friction [*Delvaux and Barth*, 2010]. This function F5 varies from 0 (perfect fit) to 360 (perfect misfit) and is independent from the dimensions of the stress ellipsoid (σ_3/σ_1).

With the Right Dihedron method, which was specially designed for focal mechanism data, the two focal planes of each mechanism are considered equivalent as they define compressional and extensional dihedrons which constrain the possible orientations of, respectively, σ_1 and σ_3. There is thus no discrimination between the actual fault planes and the auxiliary planes. However, when applying a stress tensor on a focal mechanism, the two focal planes give different values for the misfit function because they are differently oriented relative to the applied stress. With the Rotational Optimization method, we determine first the best fit stress tensor on the both nodal planes of every focal mechanism. We then apply this stress tensor on all focal planes and consider as the actual fault plane; the nodal plane for each mechanism presents the smaller F5 misfit value. The data are filtered in order to keep the most compatible focal plane for each mechanism and eventually also to remove those mechanisms for which both focal planes give an angular misfit greater than 60°. A new stress tensor is then computed, using only the selected focal planes. These last two steps are repeated until both the focal plane selection and the resulting stress tensor stabilize.

Once the final stress tensor is obtained, the tectonic stress regime index R' (ranging from 0 to 1 for extensive regimes, 1 to 2 for strike-slip regimes, and 2 to 3 for compressive regimes) is defined according to *Delvaux et al*. [1997]. The orientations of the horizontal principal stresses (S_{Hmax} and S_{Hmin}) are obtained following *Lund and Townend* [2007] as corresponding to the orientation of, respectively, the greatest and the smallest axes of the ellipse obtained by intersecting the stress ellipsoid with the horizontal plane. The quality of the results is evaluated using the World Stress Map quality ranking parameter QRfmf for formal inversion of focal mechanisms, as defined in *Heidbach et al*. [2010]. The uncertainty in the results are expressed by 1 sigma standard deviations for the individual stress axes, the stress ratio R, and the derived stress regime index R'. The 1 sigma standard deviation for the horizontal stress orientations S_{Hmax}/S_{Hmin} is then determined using the uncertainties associated with the stress axes σ_1, σ_2, and σ_3 and the stress ratio R.

5.2. First-Order Stress Field

The first-order stress field is imaged by a joint inversion of all the 118 focal mechanism data present in the database for the study area (Table 2a and Figure 5a), without any separation. The σ_1 stress axis is well constrained (7.8° standard deviation), while the two other axes are less well defined (37.8° standard deviation). This is in line with the fact that the stress ratio $R = 0.01$, which indicates that the stress tensor is very close as having a revolution symmetry around σ_1 axis and thus σ_2 and σ_3 have almost the same relative magnitude and can be easily permutated. This is typical for transitional states of stress, between strike-slip and thrust faulting (transpressional regime, here with $R' = 2.01$). The average deviation between the observed and modeled slip lines is relatively high ($\alpha = 34.0$), mainly due to some outliers for which both planes have incompatible slip deviations.

The best fit focal planes present a dominant N-S orientation, with moderately to steeply inclined dip angles, moderately to weakly inclined slip lines, and slip line azimuth pointing dominantly to north and south. The slip rakes show the presence of a large amount of strike-slip faults with almost equal proportion of dextral and sinistral movements and a smaller but still significant number of thrust-faulting movements (Figure 5b).

The horizontal compression is relatively well fixed in an average NE-SW (N150°E) S_{Hmax} direction. The overall medium quality (QRfmf = C) and the narrow dispersion of the S_{Hmax} (5.6° standard deviation) indicate that this stress tensor fits relatively well the entire data set and therefore could represent a first-order stress field. However, the relatively high average deviation angle alpha and the presence of clear outliers indicate that this first-order stress field does not fit perfectly enough with the data set and is a clear motivation for further improvements by removing the outliers or separating the data into different subsets.

In a first step, with the resulting stress tensor, we filtered the noncompatible focal mechanisms (misfit function $F5 > 60$) and found that 22 focal mechanisms are incompatible with the main first-order stress field. The remaining 96 ones provide a very similar stress tensor, but with a much lower average slip deviation alpha (18.5° instead of 34°), and hence the overall quality is improved (B instead of C).

In a second step, we checked if this relative heterogeneity can be explained by regional fluctuation of the stress field and thus by the presence of second- or third-order stress fields related to the regional and local tectonic structures of the area. We used as a starting point the spatial data separation into the five large boxes as defined above.

5.3. Second- and Third-Order Stress Fields

In the following paragraphs we present for each box successively their tectonic context, the active tectonic structures, and the stress inversion results. The detailed results are given in Tables 2a and 2b, the corresponding equal-area stereoplots in Figure 5a, and the resulting stress field is represented on map view in Figure 6. Figure 5b illustrates using rose diagrams the main structural trends of the selected focal planes.

5.3.1. Northern Tunisia (Box 1)

The Tell/northern Tunisia area (Box 1) corresponds to a fold-and-thrust belt which is part of the Maghrebides chain. This collision front is dominated by thrusting on NE-SW faults [*Rouvier*, 1977]. The Triassic rocks of the NE trending Diapirs zone mark the front of the Tell thrust sheet zone. It is composed of diapiric folds which formed during the upper Tortonian contraction and have been accentuated during the Quaternary compressive phase [*Rouvier*, 1977; *Ben Ayed*, 1993; *Meghraoui and Pondrelli*, 2012]. The eastern part of the

box is occupied by the Gulf of Tunis and its surroundings, which form a complex tectonic domain characterized by grabens limited by NW-SE to N-S normal faults (e.g., Mateur and Grombalia), NE-SW reverse faults, and E-W trend striking faults [*Ben Ayed*, 1993]. These structures, originated during late Miocene, are reactivated according the same directions during the NNW-SSE compressive Quaternary episode [*Philip et al*., 1986]. The Gulf of Hammamet consists essentially in NE-SW reverse faults associated with folds of similar orientation [*Ben Ferjani et al*., 1990; *Boccaletti et al*., 1990]. This thrust fault system, which forms an active part of the Maghrebian fold-and-thrust belt since the Tortonian [*Ben Ayed*, 1993], is interrupted by NW-SE trending Neogene grabens (Figure 1).

These current deformations mainly occur along NE trending thrust faults which have been evidenced by reflection seismic campaigns [*Gueddiche et al*., 1992, 1998] in the Tell and Diapirs zones. Known active faults in this region are often associated in a network of E-W dextral and N-S sinistral conjugated strike-slip systems [*Rouvier*, 1977; *Ben Ayed*, 1993]. These directions correspond to the two nodal planes of the majority of focal mechanisms in this box, and it is not possible on the basis on the active fault map to determine which of the two the focal planes is the actual fault plane. In the Gulf of Tunis and its adjacent areas, the structural complexity is reflected in the heterogeneity of focal mechanisms in terms of both type and orientation of the kinematic axes (Figure 2). The events 20 and 21 (Figure 2) show a local extension of oblique-normal faulting type, controlled by the reactivation of the NW-SE and still active Hammamet-Monastir N-S fault. This latter borders on its eastern side the Grombalia graben, which extends into the Gulf of Hammamet [*Kamoun et al*., 1980; *Sorel et al*., 1983; *Chihi*, 1992].

Most of the 26 focal mechanisms are characterizing Northern Tunisia of compressive type (12 data). The rest are of strike-slip to oblique-reverse type with NW-SE S_{Hmax} directions and some normal focal mechanism in the Gulf of Tunis region (Figure 3). A first and dominant stress tensor was computed on 19 data (Figure 5), giving a clear compressional regime, with a stress regime index $R' = 2.43 \pm 0.17$ and a subhorizontal principal compression (S_{Hmax}) oriented N150°E ± 12.8°. The average slip deviation alpha is 10.0°, and the quality of the result is excellent (A). The selected focal planes are moderately to steeply inclined (50–80°), with no clear preferred orientation. Rake angles indicate dominant oblique reverse movements (Figure 5b). Despite the thrust-faulting regime, the dip angle of the activated focal planes are relatively steep, suggesting that the most events reactivate existing high-angle fault planes rather than occurring along mechanically optimal low-angle thrust faults.

The seven rejected focal mechanisms (events 17, 18, 20, 21, 22, 28, and 45) are all found compatible with a secondary (third-order) stress tensor characterized by a transtensional regime ($R' = 0.92 \pm 0.12$) and N-S extension (N95°E ± 1.9° S_{Hmax}). Except for event 45, they are all distributed along an arc centered on the Gulf of Tunis on the northeastern margin of block 1, an area described above with a structural complexity and heterogeneous focal mechanisms.

5.3.2. North-South Axis (Box 2)

In central Tunisia, a fold belt limited by an important submeridian basement tectonic line forms the "North-South Axis" [*Richert*, 1971; *Burollet*, 1991]. The North-South Axis corresponds to a deep fault system that acts as a structural high characterized by tilted blocks, gaps in sedimentation, and reduced or condensed sequences [*Burollet*, 1991]. This structure limits a collapsed block to the east, affected by a few large Quaternary folds and corresponding to the Sahel Plateau. On the Bouguer anomaly map [*Jallouli and Mickus*, 2000], the deep-seated basement feature of the North-South Axis represents a steep gradient zone, and the offset near Kairouan may be clearly seen. During the NW-SE trending late Miocene and Quaternary compressive periods, this tectonic line was activated as a sinistral strike-slip fault associated with east verging thrust mostly in their northern part [*Richert*, 1971; *Ben Ayed*, 1993].

Inversion of the eight focal mechanisms present in this box gives a transpressional, slightly compressive stress tensor ($R' = 2.05 \pm 0.11$) with an E-W S_{Hmax} (N092°E ± 8.9). A good (B) quality is obtained. The relatively small number of data force the quality down to B, but the small average slip deviation ($\alpha = 5.4°$) shows that this stress tensor is well constrained. The majority of the focal mechanisms boxes have N-S trending focal planes, which suggests a directional control by the reactivation of submeridian faults which form the dominant tectonic feature in this box. The selected focal planes are moderately inclined, the slip lines are pointing either to the east or to the west, and the rake angle shows that the majority of the focal planes are oblique slip.

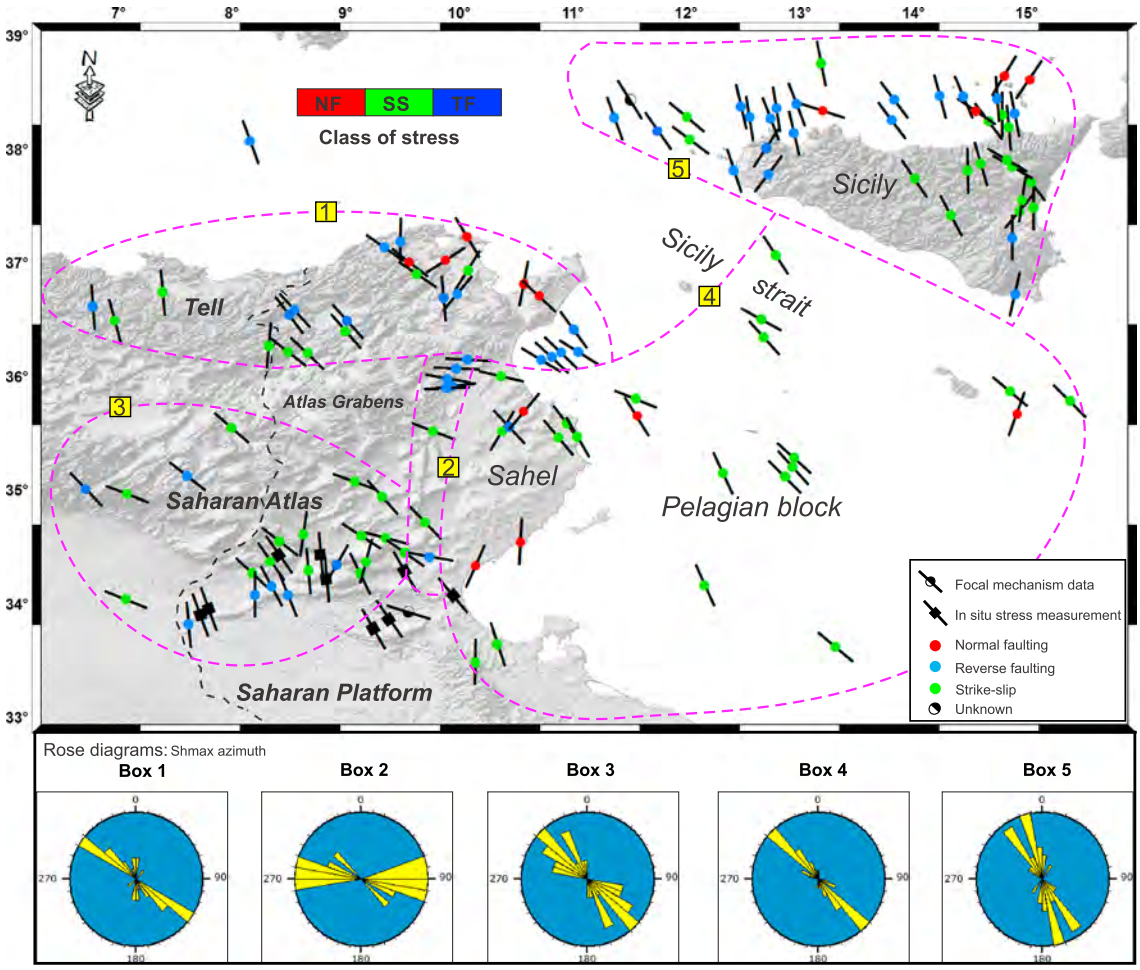

Figure 3. S_{Hmax} axis of focal mechanism data represented in this work. A color-coded central circle indicates the stress type. Rose diagrams at the bottom show the distribution of S_{Hmax} orientations in each box.

5.3.3. Saharan Atlas (Box 3)

The Saharan Atlas (Algeria/Tunisia) is essentially the morphological expression of Eocene to Quaternary intraplate deformation [*Ben Ayed*, 1993; *Bracène and Frizon de Lamotte*, 2002]. This Atlassic foreland is characterized by NE-SW folds formed during the Tortonian to Quaternary compression phase, associated with N80-120°E dextral and N-S sinistral strike-slip faults [*Philip et al*., 1986; *Ben Ayed*, 1993; *Swezey*, 1996]. It is a seismically active area with the most significant seismic activity located mainly along the N120/N140°E strike-slip faults of the Gafsa-Metlaoui region [*Saïd et al*., 2011; *Ousadou et al*., 2014; *Bahrouni et al*., 2014] and along N-S or E-W trending faults in the northern part of this domain [*Ben Ayed*, 1993]. The Gafsa-Metlaoui fault corridor was reactivated by right-lateral slip during several seismic events [*Bahrouni et al*., 2014]. This foreland is bounded by the South Atlassic front (Figure 1) and an ancient Paleozoic deep fault system [*Bracène and Frizon de Lamotte*, 2002; *Ben Ayed*, 1993; *Meghraoui and Pondrelli*, 2012]. In Tunisia, this Atlassic front corresponds to an en echelon succession of folds (northern Chott belt), developed along a large E-W basement tectonic line recognized by geophysics [*Swezey*, 1996]. This South Atlassic line separates the Atlas belt from the vast and stable Saharan platform. During the Quaternary, neotectonic activity along this major line is expressed by E-W and NW trending strike-slip and reverse faulting [*Ben Ayed*, 1993; *Harbi et al*., 1999; *Bracène and Frizon de Lamotte*, 2002; *Sébrier et al*., 2006].

The current faulting reactivation is expressed by NW-SE to E-W trending focal planes of strike-slip events in Gafsa area and focal planes of compressive solutions aligned with the N80°E trend of the northern Chott and South Atlassic tectonic line (Figure 2). Further south, the Saharan platform is almost totally devoid of seismic activity.

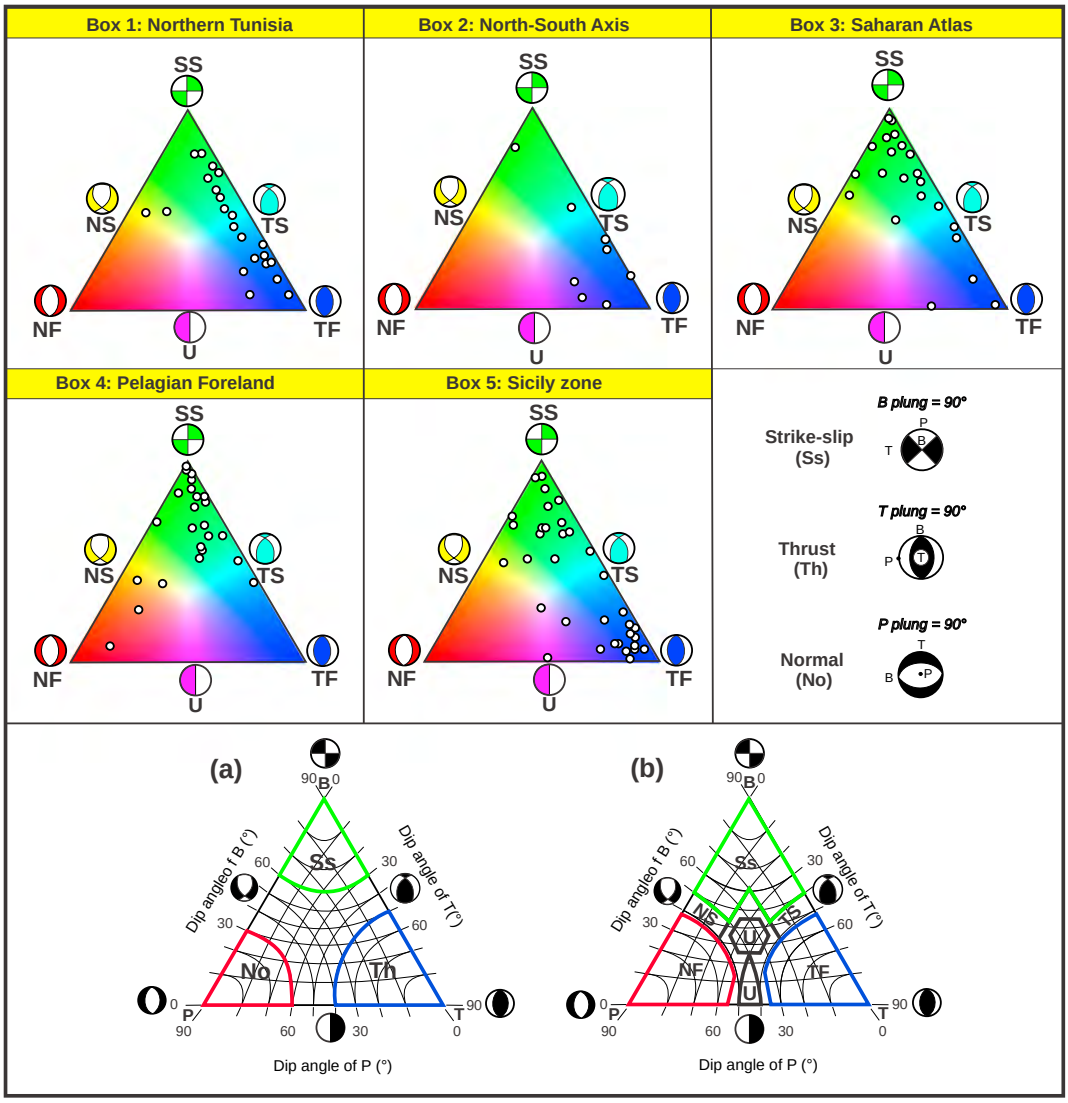

Figure 4. Representation of the kind of focal mechanisms as a function of the orientation of the *P*, *B*, and *T* axes in the triangular diagram. (a) Thrust (Th), strike slip (Ss), and normal (No) faulting as defined by *Frohlich* [1992]. (b) Thrust faulting (TF), thrust to strike slip (TS), strike slip (SS), normal to strike slip (NS), and normal faulting (NF) class as defined by *Zoback* [1992] used in the World Stress Map.

The 22 focal mechanisms of this box are dominantly of strike-slip type (SS), some oblique-slip and reverse types (Figures 2 and 3). Their inversion provides a B quality transpressional stress tensor ($R' = 2.04 \pm 0.16°$) with a N149°E ± 4.2° S_{Hmax}, consistent with the results of in situ stress measurements (Figure 3) performed in the Chott area [*Schäfer*, 1980; *Swezey*, 1996]. Most of the selected focal planes are sinistral strike slip. Two oblique focal mechanisms had to be rejected (nearby events 33 and 88 in the middle of the box), both focal planes having slip deviations above 100°.

5.3.4. Pelagian Foreland (Box 4)

The Pelagian Block includes the Tunisian Sahel and the Pelagian Sea platform [*Burollet*, 1991]. The Tunisian Sahel is affected by Quaternary NE-SW folds of large radius of curvature, associated with E-W dextral and N-S sinistral strike-slip faults [*Kamoun et al.*, 1980; *Ben Ayed*, 1993; *Chihi*, 1992; *Bahrouni et al.*, 2014]. This foreland is bounded to the east by the Malta escarpment, a NNW-SSE trending line that expands southward from southeastern Sicily over a length of about 300 km and which separates the Pelagian continental crust from the Ionian Mesozoic oceanic crust [*Argnani*, 2009; *Mastrolembo Ventura et al.*, 2014]. On the northern side of this box, during Neogene-Quaternary, the Sicily Channel has been affected by

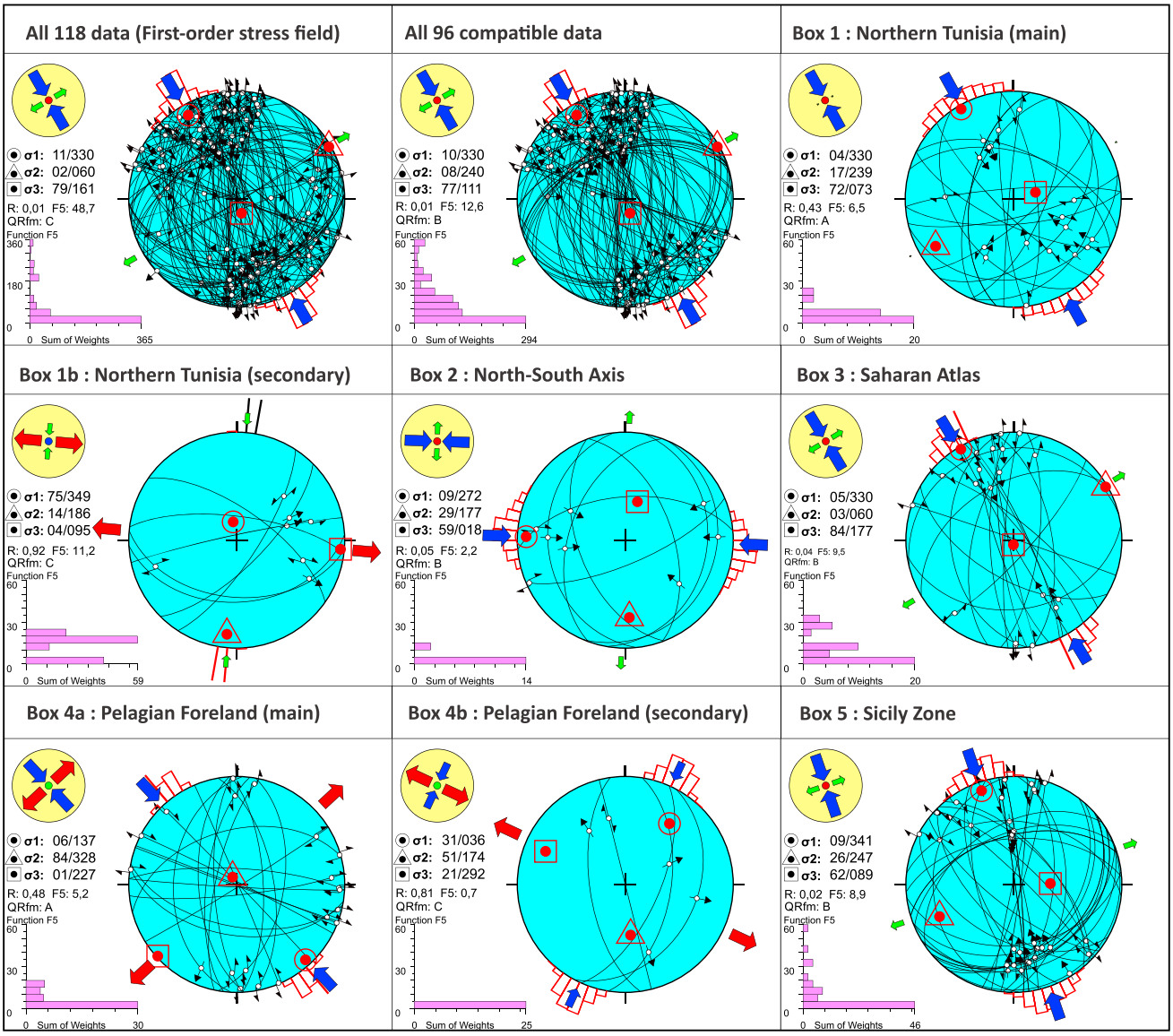

Figure 5. (a) Stress inversion and focal plane selection results: lower hemisphere equal-area stereoplots of the selected focal planes with the three principal stress axes, horizontal stresses S_{Hmax} and S_{Hmin}, distribution of uncertainties, and their 1 sigma standard deviation of the S_{Hmax} directions. Stress symbols show the horizontal stress axes (S_{Hmax} and S_{Hmin}), in function of the stress ratio *R*. Their length and color symbolize the horizontal deviatoric stress magnitude, relative to the isotropic stress (σ_i). Red outward arrows: σ_3 stress axis, green arrows: σ_2 stress axis (outward when extensional ($\sigma_2 < \sigma_i$) and inward when compressional ($\sigma_2 > \sigma_i$)), and blue inward arrows: σ_1 axis (σ_i: isotropic stress). The vertical stress (σ_v) is symbolized by a solid circle, red for extensional regimes ($\sigma_1 \sim \sigma_v$), green for strike-slip regimes ($\sigma_2 \sim \sigma_v$), or blue for compressional regimes ($\sigma_3 \sim \sigma_v$). The histogram on the lower left corner of the figures represents the distribution of the misfit function F5. F5–misfit function and QRfm–quality ranks of focal mechanism inverted. (b) Stress inversion and focal plane selection results: 10° binned rose diagrams for the selected focal planes: dip angle and strike of the focal planes, plunge angle and azimuth of the slip lines, and rake angle of the associated slips.

continental rifting [e.g., *Mastrolembo Ventura et al*., 2014] which produced the Pantelleria, Linosa, and Malta grabens, controlled by NW trend subvertical normal faults clearly seen in seismic profiles [*Civile et al*., 2010]. Some of the fault systems bordering these NW-SE passive rifts [*Argnani and Bonazzi*, 2005] have been rejuvenated as strike-slip faults during the Pleistocene compression phase [*Winnock and Bea*, 1979; *Ben Ayed*, 1993; *Serpelloni et al*., 2007; *Gharbi et al*., 2014]. The offshore Pelagian Plateau has a low frequency of seismicity with earthquakes of low to moderate magnitude [*Serpelloni et al*., 2007].

This area contains a large proportion of strike-slip (SS) focal mechanisms, with also some oblique-normal (NS) ones (Figure 2 and Table 1). During the inversion and separation process, we isolated a dominant stress tensor,

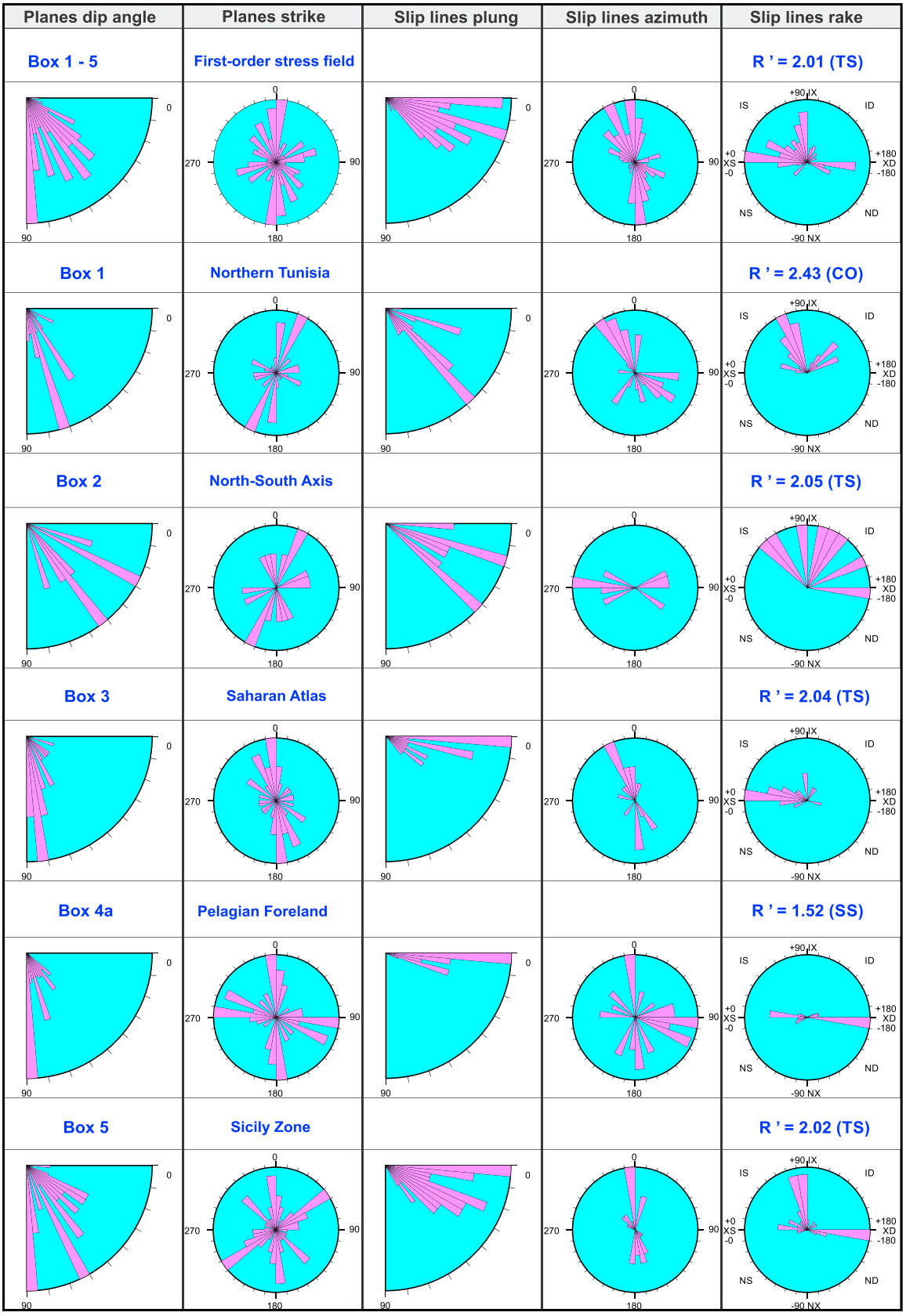

Figure 5. (continued)

Table 2a. Stress Inversion Results (Parameters of the Stress Tensor)[a]

Box Definition			Reduced Stress Tensor Parameters												Misfit and Quality Rank		
				Stress Axis σ_1			Stress Axis σ_2			Stress Axis σ_3			Stress Ratio				
No.	Location	Data	Used Data	Pl	Az	*StDev*	Pl	Az	*StDev*	Pl	Az	StDev	R	StDev	Alpha (deg)	F5	QRfmf
1–5	Tunisia/Sicily	118	118	11	330	*7.8*	2	61	*37.8*	78	163	*37.8*	0.01	0.07	34.0	46.6	C
1–5	Tunisia/Sicily	118	96	10	331	*7.6*	8	240	*31.3*	77	111	*31.5*	0.01	0.09	18.5	53.6	B
1a	Northern Tunisia	26	19	4	330	*15.3*	17	238	*20.9*	73	72	*17.4*	0.43	0.17	10.0	6.5	A
1b			7	74	350	*22.2*	15	187	*22.2*	4	95	*2.9*	0.92	0.12	10.4	11.2	C
2	North-South Axis	8	8	9	272	*13.2*	27	177	*9.2*	59	17	*11.9*	0.05	0.11	5.4	2.2	B
3	Saharan Atlas	22	20	5	330	*10.5*	3	60	*5.73*	84	177	*10.5*	0.04	0.16	15	9.5	B
4a	Pelagian Block	25	20	6	137	*15.1*	84	328	*14.6*	1	227	*5.6*	0.48	0.25	9.1	5.1	A
4b			5	31	36	*16.4*	51	174	*16.7*	21	292	*7.3*	0.81	0.31	2.2	0.7	C
5	Sicily zone	37	36	9	341	*10.5*	26	247	*26.2*	63	88	*25.6*	0.02	0.10	14.6	8.8	B

[a]Box definition: box number, location, and number of data in the box; number of data used in stress tensor solution, parameters of the reduced stress tensors: plunge (Pl), azimuth (Az), and 1 sigma standard deviation (StDev) of the principal stress axes (σ_1, σ_2, and σ_3); and stress ratio (R) and its 1 sigma standard deviation (StDev), misfit, and quality rank: average deviation between observed and modeled slip directions (alpha), minimization function F5, and quality rank for the stress inversion of focal mechanisms (QRfm) as defined in the World Stress Map.

representing 20 mechanisms (Figure 5, tensor 4a). It shows a pure strike-slip stress regime ($R' = 1.52 \pm 0.25°$), with a NW-SE (N136°E ± 4.8°) S_{Hmax}. It is represented by subvertical strike-slip focal planes with sinistral N-S and dextral E-W planes. The obtained stress field is in accordance with in situ stress measurements performed in NW Libya and SW Tunisia [*Schäfer*, 1980] and with the average S_{Hmax} orientation on the World Stress Map (WSM, 2010).

A secondary stress tensor (4b) was obtained on the remaining five focal mechanisms with four of them located along the margin of the North-South Axis (events 2, 4, 85, and 86) and one on the eastern side of the block (event 94). It has a C quality because of its small number of data but is relatively well constrained. It displays a relatively oblique extensional stress tensor ($R' = 1.20 \pm 0.21$) with a WNW-ESE horizontal extension (N25°E ± 8.3° S_{Hmax}). It dominated by N-S focal planes with dextral and normal slips. Although the stress inversion result is constrained by only five data and has to be considered with care, this suggests an influence of the prominent N-S structure of the adjacent North-South Axis, and therefore, it could also correspond to a local third-order stress perturbation.

5.3.5. Sicily Zone (Box 5)

Within Sicily Island, the tectonic setting is mainly determined by the predominance of WNW-ESE faults on its western side and ENE-WSW faults on its eastern side. These fault systems are activated with a dextral strike-slip component along a WNW-ESE direction [*Grasso et al.*, 1992; *Nigro*, 1998; *Lavecchia et al.*, 2007; *Argnani*, 2009]. The north of the island is occupied by the Maghrebides collisional front, in the eastern continuation of the North African Maghrebides belt. It is affected by a series of E-W dextral wrench faults, aligned with

Table 2b. Stress Inversion Results (Parameters of the Stress Map)[a]

Box Definition		Tectonic Regime			Horizontal Stress Axis	
No.	Region	Regime	*R'*	*StDev.*	S_{Hmax}	*StDev.*
1–5	Tunisia/Sicily	TS	2.01	*0.07*	150	*5.6*
1–5	Tunisia/Sicily	TS	2.01	*0.09*	151	*5.1*
1a	Northern Tunisia	CO	2.43	*0.17*	150	*12.8*
1b		TN	0.92	*0.12*	95	*1.9*
2	N-S Axis	TS	2.05	*0.11*	92	*8.9*
3	Saharan Atlas	TS	2.04	*0.16*	149	*4.2*
4a	Pelagian Block	SS	1.52	*0.25*	136	*4.8*
4b		UF	1.19	*0.31*	24	*6.1*
5	Sicily zone	TS	2.02	*0.10*	161	*8.3*

[a]Box definition as above, tectonic regime (TS: transpressional, TN: transtensional, CO: compressional, SS: strike slip, and UF: unknown), stress regime index (R') and its 1 sigma standard deviation (StDev), and horizontal stress axis: most compressional axis (S_{Hmax}) and its 1 sigma standard deviation (StDev).

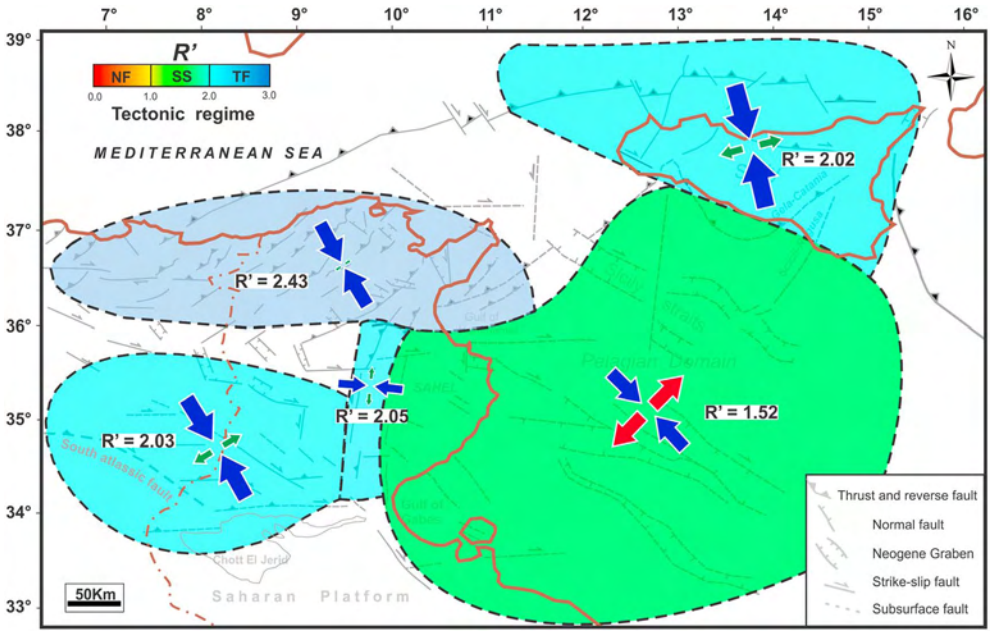

Figure 6. Sketch of the modern tectonic regime of Tunisia and its surrounding from the stress inversion results for each box.

the Azores transform fault [e.g., *Buforn et al*., 2004; *Serpelloni et al*., 2007]. The northern side of the island is part of a large E-W trending dextral shear zone, with synthetic NW-SE/E-W oriented faults, and antithetic sinistral N-S/NE-SW faults active since the Pliocene [*Orioli et al*., 2009]. The foreland of this chain is occupied by a series of NE trending folds similar as those of the Tunisian Atlas [e.g., *Montone et al*., 2004]. The western side of Sicily is characterized by several NE-SW to E-W trending thrusts and E-W to NW-SE strike-slip faults [*Giunta et al*., 2009]. The region comprised between Sicily mainland and southern Tyrrhenian Sea (Figure 1) is characterized by a south verging thrust and fold belt [*Accaino et al*., 2011].

The focal mechanisms are of thrust faulting type offshore northern Sicily with E-W focal planes and become more strike slip toward the interior of the island, with NW-SE and NE-SW focal planes (Figure 2). The result of the inversion (B quality) shows an almost pure transpressional stress tensor ($R' = 2.02 \pm 0.10$) with a NNW-SSE S_{Hmax} (N161°E ± 8.3°). The selected focal planes are a combination of relatively low-angle thrust planes trending ENE-WSW to E-W and high-angle strike-slip planes trending N-S and NE-SW.

6. Tectonic Regime and Focal Depth Distribution in Tunisia

The most conspicuous characteristic in the focal mechanism distribution in Tunisia is their depth dependence. The shallow part of the seismogenic zone is characterized by a mix of reverse and strike-slip faulting earthquakes, while a pure strike-slip faulting regime dominate at depth [*Imanishi et al*., 2011]. To illustrate study the depth dependence of earthquakes in the Alpine belt and intracontinental Atlas, we use the crustal structure across Tunisia according to *Jallouli and Mickus* [2000], who divided the region into several zones of different crustal features taking into account the Moho depth [e.g., *Ben Ferjani et al*., 1990; *Buness et al*., 1992; *Grad and Tira*, 2009]. On a N-S crustal section through the structural domains of Tunisia (Figure 7b), the focal mechanisms are plotted with their type in the Frohlish Triangle (Figure 7a) in order to better identify and characterize the different Tunisian seismogenic areas:

1. In the north, below the allochthonous contacts units and within the Triassic diapirs domain, seismicity is concentrated in the upper crust with predominance of compressive and transpressive focal mechanisms. This is due to the reactivation of thrust and reverses faults that formed in the Tortonian and continued to be active during the Quaternary [*Rouvier*, 1977; *Philip et al*., 1986; *Gueddiche et al*., 1992]. This kind of seismic activity is a characteristic for convergence domains with a thin crust and a relatively shallow Moho [e.g., *Serpelloni et al*., 2007; *Artemieva and Thybo*, 2013].

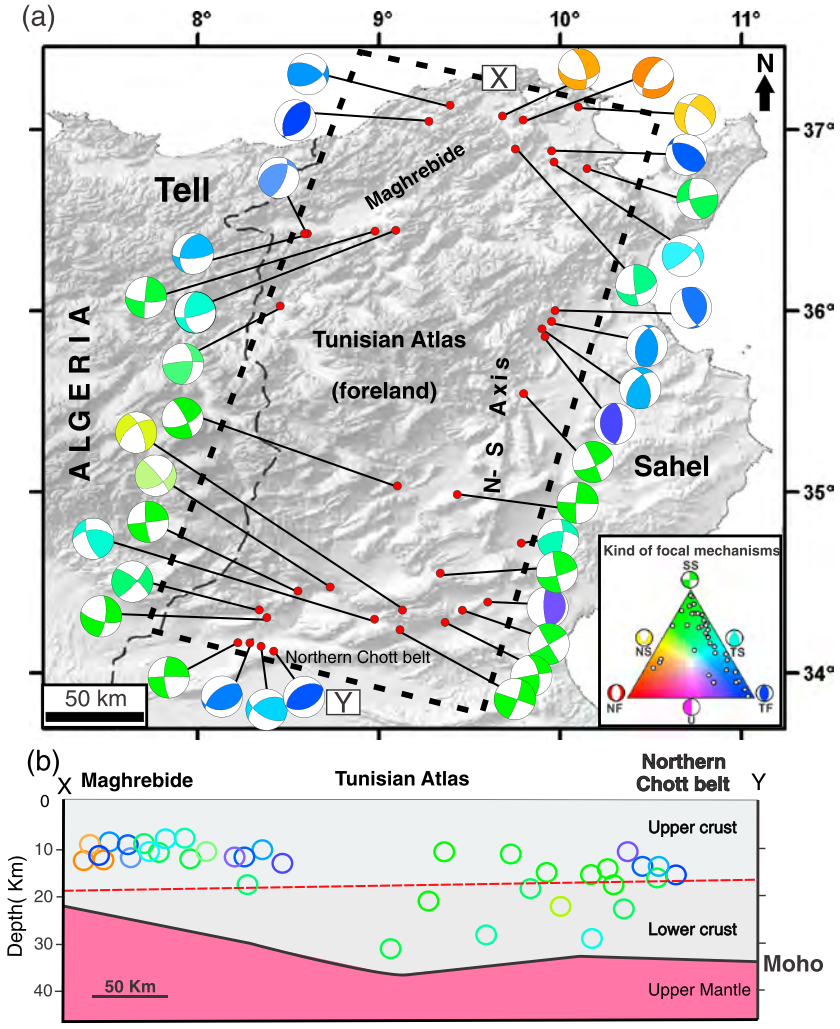

Figure 7. (a) Spatial distribution of focal mechanism solutions in different tectonic domains, where different colors are used to differentiate reverse (blue), strike-slip (green), and normal (red) faulting mechanisms. Each focal mechanism is plotted by white circle (below right) on the triangle diagram [*Frohlich*, 1992]. (b) Types of estimated focal mechanism solutions in the *X-Y* cross section (Geotraverse data in *Jallouli and Mickus* [2000]), where the color is based on the triangle diagram in Figure 7a. The focal mechanisms are represented in the lower hemisphere projection.

2. The seismogenic zone corresponding to the Atlassic foreland shows the predominance of strike-slip earthquakes in the lower crust. In southern Atlas, strike-slip focal mechanisms are dominant probably due to the reactivation of ancient deep faults (Gafsa, Metlaoui, Ben Aoun; northern Chott belt…) recognized by geophysics [e.g., *Ben Ferjani et al.*, 1990; *Zouaghi et al.*, 2005] and reactivated during the Quaternary [*Zargouni and Ruhland*, 1981; *Ben Ayed*, 1993; *Swezey*, 1996; *Bahrouni et al.*, 2014; *Gharbi et al.*, 2014]. Only three compressive focal mechanisms appear in the blind thrust front that delimits southern Atlas and was apparently activated during the Pliocene-Quaternary period [*Vially et al.*, 1994].
3. On the southern side, the central Atlas graben is a paraseismic zone (Figure 2) characterized by low seismicity (frequency and magnitude). Only a few earthquakes affecting the lower crust are associated with E-W and N-S major faults (Figures 1 and 2), inherited from the Cretaceous tectonic activity [*Ben Ayed*, 1993] and reactivated in the Quaternary [*Philip et al.*, 1986; *Ben Ayed*, 1993; *El Ghali et al.*, 2003]. This area with the deepest Moho and a thick and rigid continental crust [*Jallouli and Mickus*, 2000] appears to have resisted to the seismogenic deformation. With the presence of Neogene grabens in this area, there is a relatively low seismogenic potential which may be explained by the overall less frequency and lower magnitude of normal-fault earthquakes in the continental crust as compared to strike-slip and thrust faults [*Jackson*, 1987; *Axen*, 2007].

The fact that 90–100% of the Africa-Europe current convergence is accommodated in the Maghrebides chain [*Nocquet and Calais*, 2004; *Serpelloni et al*., 2007] may explain the relatively high rate of shallow seismicity in northern Tunisia. In the Atlassic foreland, the majority of intracontinental deformation within the crust and hence intraplate seismicity is accommodated by reactivation of preexisting faults [*Coward*, 1994] and causes variations local stress concentration [*Campbell*, 1978].

7. Discussion

The focal mechanisms of the Tunisia-Pelagian Plateau-Sicily area show a significant variability among the populations analyzed, with faulting type ranging from purely reverse to purely normal under laterally variable tectonic stresses. This represents potential fault interactions and local stress transfer in an area of distributed tectonic activity. The main outcome of this study is that the relative heterogeneity of the focal mechanisms in the study area can effectively be explained by a regional fluctuation of the stress field as observed in the five boxes. A total of four second-order and three third-order stress tensors are obtained, which explain all but 5 of the 118 focal mechanisms compiled. These stress tensors have average misfit angles between 2 and 14°, much less than the average 34° for the first-order tensor, for which also 25 data are incompatible. The apparent heterogeneity in the focal mechanisms of the Tunisia-Pelagian Plateau-Sicily area is better explained in terms of second- and third-order stress fields influenced by the regional and local tectonic structures of the area. These results validate also the large box zonation approach. We have seen that for two of the boxes, some focal mechanisms could not be explained by the second-order stress tensor computed and that the incompatible mechanisms define a small area for which a third-order stress tensor was obtained. The preponderance of N-S direction in the focal planes (Figure 5b, boxes 1–5) do not fit with the known major E-W to NE-SW structural trends in study area (Figure 1). They could therefore correspond to reactivated secondary structures

7.1. Relationship Between Seismotectonic and Neotectonic Stress Fields

Within the thrust faulting domain of northern Tunisia, the seismotectonic stress field is characterized by a stress regime index $R' = 2.43$ and a NW-SE S_{Hmax} orientation, very similar to the N160-170°E orientation of the neotectonic compression obtained from geological fault slip data [*Philip et al*., 1986; *Rebaï et al*., 1992; *Ben Ayed and Oueslati*, 1988; *Meghraoui and Pondrelli*, 2012]. Our seismotectonic observations and stress inversion results are also in agreement with the neotectonic data of *Ben Ayed* [1993], *Morel and Meghraoui* [1996], *Serpelloni et al*. [2007], *Meghraoui and Pondrelli* [2012], and *Gharbi et al*. [2014], who suggested that this part of the plate boundary acts as a transpressional deformation area, where active thrust belts are controlled by right-lateral transcurrent faults.

In the North-South Axis, the transpressional to compressional stress regime with an E-W S_{Hmax} direction that we obtained from the inversion of focal mechanism data is different from the strike-slip regime and NNW-SSE S_{Hmax} reported in neotectonic studies [*Richert*, 1971]. The obtained S_{Hmax} orientation rotates almost 40°W clockwise relative to the surrounding boxes, becoming perpendicular to the north trending thrust belt. The cause for this third-order stress perturbation is unclear and might be related to the ancient submeridian orientation of the ancient thrust belt that it reactivates. In the Tunisian Saharan Atlas, the NW-SE and E-W trending conjugate that strike-slip fault system was active during Pleistocene-Holocene [*Zargouni and Rhuland*, 1981; *Saïd et al*., 2011; *Gharbi et al*., 2014]. The current stress field deduced from the formal inversion of focal mechanisms is in agreement with the paleostress results obtained for the Pleistocene. The northern Chott, which is part of the Atlas blind thrust front, was affected by tectonic compression during the Quaternary [*Ben Ayed*, 1993; *Swezey*, 1996] and appears also presently active with a NNW-SSE S_{Hmax} in a compressional to transpressional regime. East of the North-South Axis, the Sahel/Pelagian Plateau, which subsided during the Oligocene extensional period [*Burollet*, 1991], is characterized by a strike-slip setting with a NW-SE S_{Hmax} direction and was still active during the historic period [*Sorel et al*., 1983]. In the northern and northeasten sides of Sicily, major events rupturing E-W and NW-SE reverse and normal faults have repeatedly caused damage during historical and recent periods [*Valensise and Pantosti*, 1992]. The most destructive ones are the 1693, M_w 7.4 Hyblean and the 1908, M_w 7.1 Messina Strait earthquakes [*Bianca et al*., 1999]. This shows that the N-S to NE-SW trending stress field is almost stable since Quaternary to present-day with a few third-order perturbations.

7.2. SH Orientations and Tectonic Regime Variations

Our results evidence a spatial distribution of orientation, kinematics, and active tectonic regime for the central Mediterranean Africa-Eurasia plate boundary. We evidence a change in the current tectonic regime from compressional to transpressional in the Tunisian Maghrebides and Atlas areas, to strike slip/transtansional in the Pelagian foreland, with rather homogenous S_{Hmax} orientations. The building of the compressional belt along this part of the Maghrebides chain produced a tectonic inversion by a compressional reactivation of the NE-SW and E-W trending basin margins [*Ben Ayed*, 1993; *Morel and Meghraoui*, 1996; *Billi et al*., 2011]. The Europe-Africa contractional deformation in central Mediterranean is mostly accommodated in the southern Tyrrhenian region [*Billi et al*., 2011; *Palano et al*., 2012; *Nocquet*, 2012; *Pierdominici and Heidbach*, 2012] with a NNW-SSE S_{Hmax} by reactivating E-W trending thrust/back-thrust systems. Geodetic and seismotectonic data indicate that this compressive domain is adjacent to a NW-SE extension domain in the Messina Straits/eastern Sicily [e.g., *Argnani*, 2009; *Serpelloni et al*., 2013; *Nocquet*, 2012]. This block rotates clockwise around a pole positioned off Cyrenaica [*Nocquet*, 2012] and is separated from the African plate by the extensional Sicily Channel area [*Argnani*, 2009]. Within the African plate, a continent-ocean transition formed during the subduction event between the Ionian oceanic lithosphere and the continental lithosphere of the Sicily/Pelagian domain [*Faccenna et al*., 2007]. It could be responsible for these two different tectonic regimes along the convergent boundary. In the Tunisian Atlas and Pelagian Shelf, it is essentially the preexisting NW-SE to E-W strike-slip system which is reactivated.

The average orientation of S_{Hmax} in the study area roughly corresponds to the direction of plate convergence for the central Mediterranean plate boundary [*Sella et al*., 2002; *Serpelloni et al*., 2013; *Ousadou et al*., 2014]. The studied compressive plate boundary is fragmented and interrupted by zones of less homogenous and more distributed tectonic deformation with a spatial variation of tectonic regime from north to south and east to west mainly expressed by stress axes permutation (Figure 6). Except for the North-South Axis (box 2) and the two marginal regions of boxes 1 and 4 on which we evidence a third-order stress perturbation, the S_{Hmax} stress directions are fairly constant over large areas, with a slight clockwise rotation in Sicily relative to the rest of the region, while the stress regime is fluctuating from a pure strike-slip regime in the Pelagian Block to a pure compressional regime in the Maghrebides chain. We suggest that, except for the preexisting third-order heterogeneities, the current tectonic and kinematic parameters are still controlled by the oblique Africa-Eurasia plate convergence. The observed strain field and tectonic deformations are largely subsurface responses to the internal dynamic processes as illustrated in Figures 8 and 9. The N-S trending transtensional belt running along eastern Sicily and Maltese Escarpment (Figure 8) constitutes the transition zone between the "northern Africa" plate boundary region (shown here by the South Tyrrhenian seismic belt) and the Calabria-Ionian region, characterized by extension [*Serpelloni et al*., 2013].

In the Pelagian Shelf and Sicily zone, *Serpelloni et al*. [2007] documented a distributed deformation accommodating almost 1.5 mm/yr of NE-SW extension along the Sicily Strait, 1.7 mm/yr of right-lateral movement in the NW-SE trending of eastern Tunisia-Libya strip, and 2.1 mm/yr of northwestward rift of Sicily in the southern Tyrrhenian compressive belt. In the context of the dominant NW right-lateral movements associated with local WNW-ESE extension in the graben system, the Pelagian Block and the Tunisian Sahel act as a specific strike-slip to transtensional tectonic domain in central Mediterranean. This transtensional region of second order, with a total absence of reverse focal mechanism, is bordered by compressive belts (the North-South Axis and Maghrebian fold-and-thrust belt) and the Maltese Escarpment and Medenine fault system (Figure 8). Separated by these deformation belts, the Pelagian-Tunisian Sahel block is relatively independent with respect to the Africa and Eurasia motions.

7.3. Relation to Slab Deformation

Based on our results and previous works, we relate the surface deformation and kinematics of the study area to the geodynamic and internal dynamic processes. The recent stress tectonic regime and its variations shown within the studied segment of plate boundary are most likely influenced by subduction traces and internal dynamics beneath the complex mobile belts. The inversion of focal mechanisms in northern Tunisia and South Tyrrhenian/Sicily area shows an average NNW trending compressional to transpressional stress regime which reactivates inherited structures (thrusts/back thrusts/oblique faults) mostly formed as a consequence of slab detachment and rollback toward the Calabrian arc (Figure 9) [*Faccenna et al*., 2007]. In the foreland (Sicily Channel/Pelagian Block), the transtensional tectonic regime is developed after the

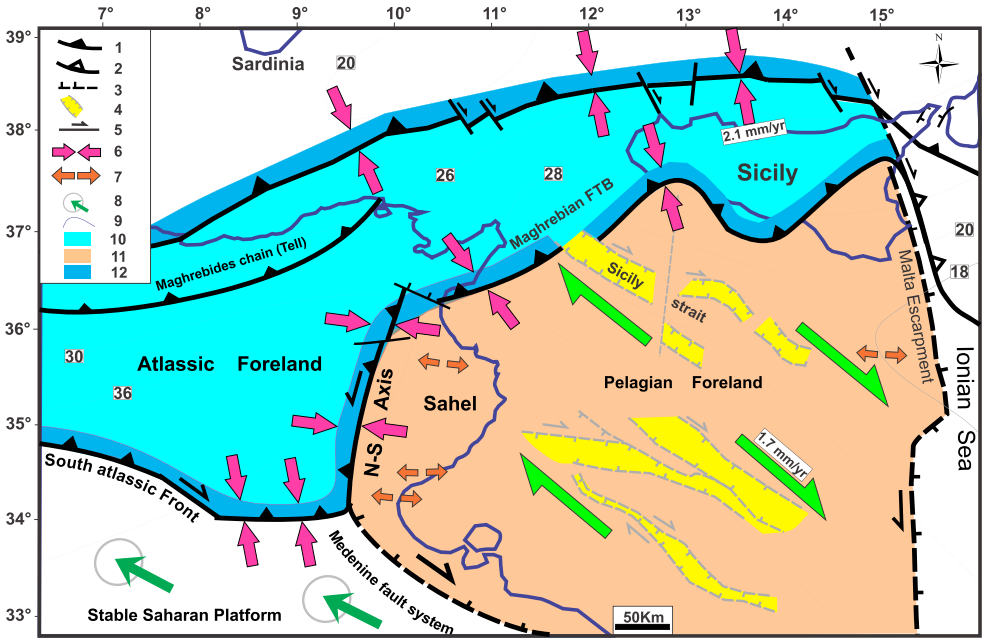

Figure 8. Sketch of current kinematics pattern of study area. 1: soft collision/thrust and reverse faults, 2: oceanic subduction, 3: normal fault, 4: neogene graben, 5: strike-slip fault, 6: compressional direction, 7: extensional direction, 8: the motion vectors of points south of the seismically active belts in northern Africa [*Serpelloni et al.*, 2007], 9: depth to the Moho discontinuity [*Grad and Tiira*, 2009], 10: compressional to transpressional area, 11: strike-slip to trantensional area, and 12: compressive belt. Maghrebian FTB: Maghrebian fold-and-thrust belt.

slab segmentation 5–4 Ma ago [*Faccenna et al.*, 2004; *Billi et al.*, 2011]. It remains presently active as shown by the combination of strike-slip and extensional earthquakes. This present tectonic regime with northeastward extension may be due to the westward propagation of the slab pull effect, where slabs are still attached (i.e., Ionian or Hellenic subduction).

The stress regime changes from extensional in Messina Strait/NE Sicily [*Neri et al.*, 2009; *D'Agostino et al.*, 2011] to compressional in South Tyrrhenian/North Sicily-North Tunisia (with counterclockwise rotation). This is in line with the proposed joint action between N-S Africa-Europe convergence and eastward rollback of the Ionian subduction slab [*Negredo et al.*, 1999]. During the sinking to its present position under Calabria, the slab continued to impose a traction that may have dragged the tectonic blocks of Sicily toward the southeastern Tyrrhenian [*Mastrolembo Ventura et al.*, 2014]. This may explain the increasing of compressive earthquakes observed in the Tyrrhenian back arc. The current NE-SW extension and crust stretching accommodated across the Sicily Channel may be absorbed by southwestward horizontal shortening shown along the North-South Axis belt in Tunisia.

On the basis of existing tomographic results [*Piromallo and Morelli*, 2003; *Carminati et al.*, 1998], we suggest that the occurrence of diffuse lower crustal seismicity in the Tunisian Atlassic foreland at 15–25 km depth is due to the stress transfer toward upper plate from the shallow confined slab segment beneath Tunisia (Figure 9, cross sections B-b and A-a). This stress was released along preexistent weak zones by seismic reactivation of inherited deep strike-slip faults of Tunisian Atlas. Southward and eastward, the Tunisian slab edges are expressed at subsurface by the northern Chott and North-South Axis thrust belts, respectively (Figure 9, cross sections A-A and B-b), characterized by compressive focal mechanism. In addition, the directions of *T* axes of majorities of focal mechanisms of the crustal earthquakes are predominantly parallel to the plate boundary. This uniformity of *T* axes can be interpreted as a reaction to the buoyancy force of the lower crust caused by the rollback slab, by compressional force within the foreland (i.e., Atlas domain) perpendicular to Maghrebides collisional front. This suggestion is consistent with the interpretation of *Singer et al.* [2014] that viscous bending and stress transfer in the northern foreland of the Central Alps (related to the lateral extent of the European slab) is transformed to a compressional force in the foreland perpendicular to the Alpine front.

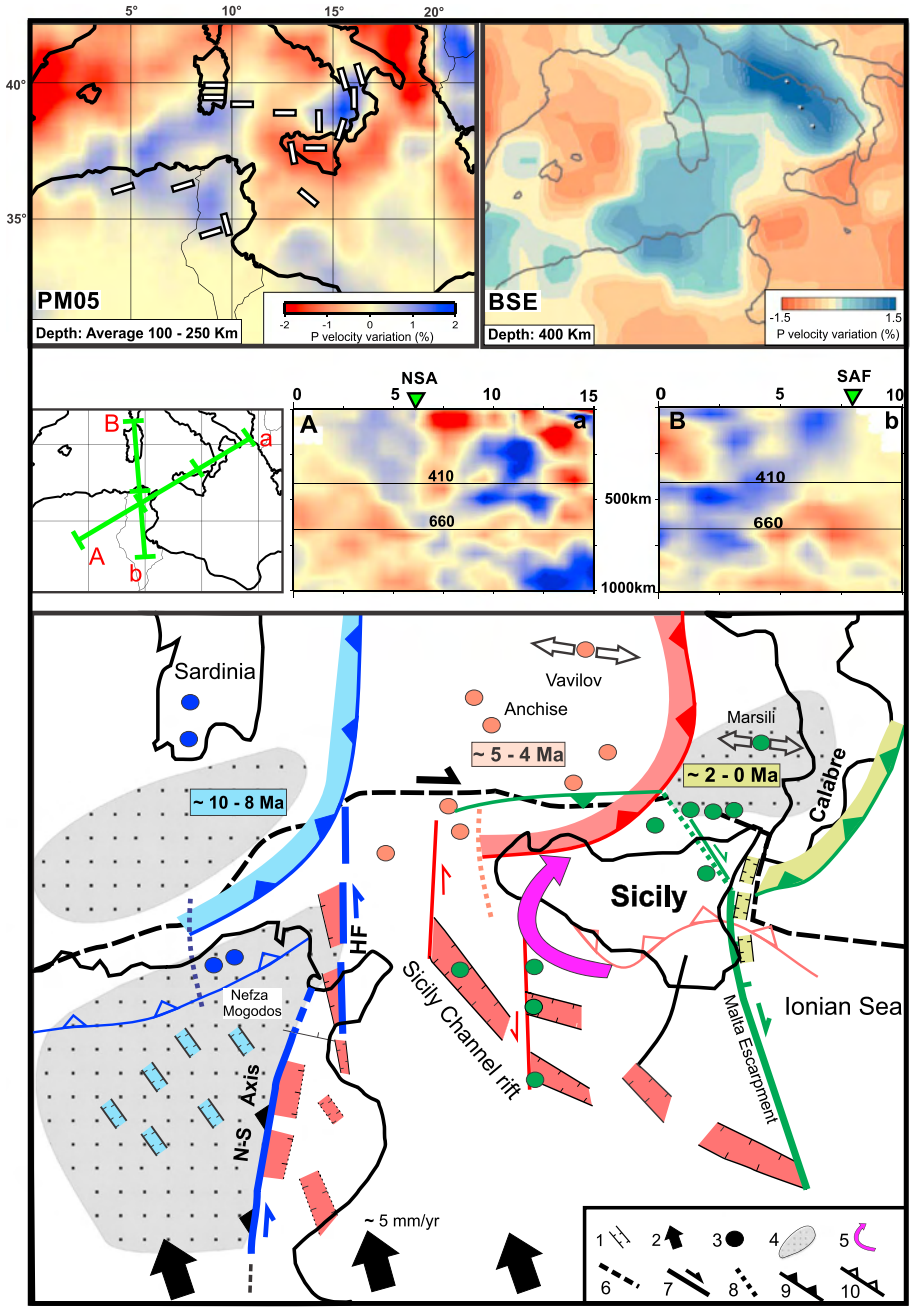

Figure 9. Reconstruction of the evolution of the main geodynamic elements in the study region, based on *Faccenna et al.* [2005, 2007, 2014], *Argnani* [2009], and *Piromallo and Morelli* [2003]. 1: graben/normal fault, 2: plate motion (Nuvel 1A [*DeMets et al.*, 1990]), 3: full circles show only volcanoes active during the different stages, 4: high-velocity anomalies at 100–250 km of depth, 5: purple arrow indicates the possible mantle flow path [*Civello and Margheriti*, 2004], 6: plate boundaries are as in *Bird* [2003], 7: STEP fault, 8: dashed lines indicate the lateral boundary between subduction-related magmatism and anorogenic, 9: subduction front colored by their deformation periods, and 10: thrust belt. Map views of tomographic results: (left) the model PM0.5 [*Piromallo and Morelli*, 2003] and (right) the model BSE [*Carminati et al.*, 1998]. The white sticks indicate SKS splitting measurements from the compilations by *Wuestefeld et al.* [2009] and *Faccenna et al.* [2014] with orientation showing the "fast axes." Tomographic cross sections are from model PM0.5. NSA: North-South Axis, SAF: South Atlassic front, and HF: Hammamet fault.

In result, the expected role of slab deformation and its evolution in central Mediterranean may drive the deformation strain, kinematics, and upper plate behavior over the study area.

7.4. Effects of Mantle Dynamics

Central Mediterranean represents the major "catchment area" where the Calabrian slab is sinking, consuming the last lithospheric vestige under the Ionian Sea [*Faccenna et al*., 2014]. The upper mantle flow pattern beneath the Tunisian Maghrebides chain and its foreland, as revealed by SKS fast splitting directions [*Faccenna et al*., 2014], is perpendicular to the *P* axis of focal mechanisms and the NW-SE S_{Hmax} orientations and is parallel to the high-velocity zone of residual slab material under Tunisia (Figure 9). This is in support to the suggestion that mantle flow pattern generated by the rollback movement of the Calabrian slab as shown by *Piromallo and Morelli* [2003] and *Lucente et al*. [2008] match closely the current extensional orientation [*Jolivet et al*., 2009]. At smaller scale, there is a number of small convection cells located at the edge of the slabs which may explain some local surface heterogeneity in the study region. In particular, in the southern part of the North-South Axis, which coincides with the eastern limits of residual Tunisian slab, the SKS fast splitting directions are reoriented in a submeridian direction (Figure 9), perpendicular to the local E-W S_{Hmax} direction. We therefore suggest that the sinking of the detached free portion of the slab beneath Tunisian area may cause flow in the viscous mantle which may lead to a third-order deflection of the crustal stress field. The third-order extensional regime observed around the Gulf of Tunis can also be due to the lithospheric removal process and upraise of sublithospheric mantle beneath the topographic highs [*Göğüş and Pysklywec*, 2008]. The latter may induce a crustal extension at small scale even in a convergent setting. The tensional stress field observed in the Sicily Channel is consistent with the 3-D model results of *Petricca et al*. [2013], following which mantle drag at the base of the lithosphere can create a vertical motion at subsurface and may explain the presence of rifting processes in a mainly convergent regime. Other SKS splitting data demonstrate the toroidal flow that is expected on the western corner of the Tyrrhenian slab within the Sicily Channel [*Civello and Margheriti*, 2004; *Faccenna et al*., 2014]. In this case we presume that this small convection cell, confined beneath the Sicily Straits where SKS fast axes turn in a N-S direction and then E-W direction (Figure 9) in the Tyrrhenian Sea [*Civello and Margheriti*, 2004], may favor a clockwise rotation of stress field from Sicily toward the Ionian domain.

At a large scale, the boundary conditions of the mantle flow computations which are characterized as shear stress free at all or most of the surface [e.g., *Zhong et al*., 2000; *Faccenna et al*., 2014] sustain the idea that the first-order transpressional stress regime shown here was guided by preexistent weak zones at plate boundaries (i.e., Africa-Eurasia). As a result, the weak control of the relative plate motion on the deformation regime in central Mediterranean proposed by *Nocquet* [2012] and *Chiarabba et al*. [2015] and upper plate interactions are not sufficient to explain the observed kinematics or present tectonic stress in our study area. Therefore, we predict that internal forces within the lithosphere and/or lithosphere-mantle interaction should contribute or even largely control the observed tectonic regime variation and stress field heterogeneities.

7.5. Role of Major Discontinuities

Combining tectonic reconstitutions, tomography data, geological, and geophysical evidence [*Jolivet and Faccenna*, 2000; *Govers and Wortel*, 2005; *Argnani*, 2009; *Lucente*, 2008], we suggest a primary role of the preexisting weak zones in the active geodynamics of the study area. Among the major weakness zones, the so-called Slab Transfer Edge Propagator (STEP) faults are lithospheric scale structures formed as subvertical tear faults during the trench retreat or slab rollback and acting as transform faults [*Govers and Wortel*, 2005]. One of them has been proposed between the north Tunisian and the Calabrian plate boundary segments, with a right-lateral motion along the oblique convergent plates (i.e., Africa-Eurasia) [*Wortel et al*., 2009]. It created a free slab portion under Tunisia and East Algeria during the Late Tortonian period and caused migration of the remnant slab eastward [*Faccenna et al*., 2007]. Around this transform fault system, we observe a mix of reverse and strike-slip focal mechanisms in the North Sicily domain and northern Tunisia (Figure 2). The first-order transpressional regime obtained for this region is in good agreement with the primary role expected by this STEP fault with right-lateral motion.

The former central Mediterranean subduction tear fault may have been intercepted by major crustal discontinuities which can act as an active STEP fault. Some of them like the Malta escarpment, N-S transfer

fault system of Sicily Straits and North-South Axis (Tunisia) which may represent trench-perpendicular tears [*Argnani and Bonazzi*, 2005; *Argnani*, 2009] which interfere directly with the plate boundary and represent a typical candidate for STEP faulting. Tomography images and cross section A-a (Figure 9) show that the STEP fault of the North-South Axis-Hammamet relay (NSAH) coincides well with the eastern limits of positive anomalies attributed to the residual slab beneath Tunisia and the western edge of slab windows of the Sicily Channel (Figure 9). For this, we propose that this N-S trending fault system is the surface expression of a vertical lithospheric tear at greater depth. The presence of syntectonic Pliocene sediments [*Ben Ayed*, 1993; *Bédir*, 1995] on top of this crustal scale fault (Figure 9) may be the result of a recent lithospheric vertical movement of this STEP fault, in response to the rollback and lateral migration of the Calabrian slab eastward. Along the southern part of this major fault system, the North-South Axis tectonic line is characterized by a complex deformation history throughout the Mesozoic-Cenozoic [*Burollet*, 1991]. The latter separates two different adjacent seismotectonic regimes: transpressional to compressional within the Tunisian Atlas toward west and strike slip to transtensional in the Sahel/Pelagian platform.

Further east, the Malta Escarpment Mesozoic weakness zone, which forms the limit between the western buoyant African lithosphere and the eastern Ionian subduction domain [*Carminati et al*., 1998], appears to play an active role in the southward propagation of the Tyrrhenian slab [*Govers and Wortel*, 2005]. This major discontinuity constitutes a limit between the extensional Messina Straits/southern Calabria area and the compressional South Tyrrhenian domain, with clockwise rotation of the maximum horizontal stress [*Neri et al*., 2009; *D'Agostino et al*., 2011]. We find that the major crustal discontinuities limiting the slab/window edge (i.e., NSAH and Malta Escarpment STEP faults) play an active role in the lateral variations/distribution of tectonic regime and stress field rotation/deviation of Tunisia and surrounding area.

8. Conclusion

Using a formal inversion of an initial database of 118 focal mechanisms, we characterize the first-, second-, and third-order stress patterns of Tunisia and surrounding area. Focal mechanism characterization using the Frohlich diagram and stress tensor inversion with the Win-Tensor program allows specifying the current tectonic stress and its spatial variations. The inversion of focal mechanisms evidence a current stress field which is relatively consistent with the neotectonic stress field determined elsewhere using fault slip data. The collisional belt of Maghrebides chain (northern Tunisia to Sicily) is characterized by shallow earthquakes concentrated in upper crust and compressional to transpressional tectonic regime causing a tectonic inversion of the NE-SW and E-W trending basin margins from extension to compression. The Atlassic and Pelagian foreland shows a predominance of deep strike-slip earthquakes located largely within the lower crust due to reactivation of inherited strike-slip systems. Today, most of Tunisia, Sicily, and the Pelagian Shelf move together with the African plate (with more specific kinematics for each of this domains), as shown by available GPS velocities and active seismic belts, matching the African plate motion.

Lateral slab migration and segmentation in central Mediterranean may drive and influence the current tectonic deformation, kinematics, and upper plate motion over the region extending from eastern Algeria/Tunisia to eastern Sicily. We predict that internal forces within the lithosphere and/or lithosphere-mantle interaction should contribute and possibly control the tectonic regime variation and observed stress field heterogeneities. In addition, we suggest that the major Slab Transfer Edge Propagator (STEP) faults (i.e., NSAH relay and Malte Escarpment), which laterally delimit the subducting slabs and are seismically active, play an active role in lateral variations of the tectonic regime and stress field deviation (second and third orders) through the Tunisian to Sicilian domains.

At the plate scale, the upper crustal stress field and tectonic regime variation in Tunisia and its adjacent areas may be governed by oblique plate convergence, the contrasting nature of the lithosphere (oceanic in the Ionian Sea and continental elsewhere), the remains of the subduction slabs, and mantle dynamics.

Our results provide additional constraints to the driving forces and geodynamic models, allowing them to better explain the current plate interactions (Africa/Eurasia) and crustal tectonic complexities in the studied central Mediterranean regions.

Acknowledgments
Moments tensors data used in this work can be found online at http://www.globalcmt.org/CMTsearch.html, www.bo.ingv.it/RCMT/searchRCMT.html, and www.emsc-csem.org. We thank Gianfranco Vannucci, Enrico Serpelloni, and Silvia Pondrelli who provided us with several moment tensors of Tunisia and its neighboring regions. Claudio Faccenna, Lopo Boshi, and Ludwig Auer are thanked for their help and encouragement. Also a great thankful to Claudia Piromallo and Eugenio Carminatti for providing the tomography data and improving the discussion of this paper. This manuscript is benefited from the constructive comments of an anonymous reviewer and the encouragement of the Editor Nathan Niemi and Associate Editors. It is a contribution to the IGCP 601 project "Seismotectonics and seismic hazards of Africa."

References

Accaino, F., R. Catalano, L. Di Marzo, M. Giustiniani, U. Tinivella, R. Nicolich, A. Sulli, V. Valenti, and P. Manetti (2011), A crustal seismic profile across Sicily, *Tectonophysics*, *508*(1), 52–61.

Angelier, J. (2002), Détermination du tenseur des contraintes par inversion de mécanismes au foyer de séismes sans choix de plans nodaux, *C. R. Geosci.*, *334*(1), 73–80.

Angelier, J., and P. Mechler (1977), Sur une méthode graphique de recherche des contraintes principales également utilisables en tectonique et en seismologie: La méthode des dièdres droits, *Bull. Soc. Geol. France*, *XIX*(6), 1309–1318.

Argnani, A. (2009), Evolution of the southern Tyrrhenian slab tear and active tectonics along the western edge of the Tyrrhenian subducted slab, *Geol. Soc. London Spec. Publ.*, *311*(1), 193–212.

Argnani, A., and C. Bonazzi (2005), Malta Escarpment fault zone offshore eastern Sicily: Pliocene-Quaternary tectonic evolution based on new multichannel seismic data, *Tectonics*, *24*, TC4009, doi:10.1029/2004TC001656.

Artemieva, I. M., and H. Thybo (2013), EUNAseis: A seismic model for Moho and crustal structure in Europe, Greenland, and the North Atlantic region, *Tectonophysics*, *609*, 97–153.

Axen, G. J. (2007), Research focus: Significance of large-displacement, low-angle normal faults, *Geology*, *35*(3), 287–288.

Bahrouni, N., S. Bouaziz, A. Soumaya, N. Ben Ayed, K. Attafi, Y. Houla, A. El Ghali, and N. Rebai (2014), Neotectonic and seismotectonic investigation of seismically active regions in Tunisia: A multidisciplinary approach, *J. Seismol.*, *18*(2), 235–256.

Bédir, M. (1995), Mécanismes géodynamiques des bassins associés aux couloirs de coulissement de la marge atlasique de la Tunisie Sismo-tectonique et implications pétrolières, Unpublished PhD thesis, University of Tunis.

Ben Ayed, N. (1993), *Evolution Tectonique de l'Avant-pays de la Chaîne Alpine de Tunisie du Début du Mésozoïque à l'Actuel*, Ann. Mines et Géol., Tunisie, vol. 32, 286 pp. [Available at https://tel.archives-ouvertes.fr/tel-01009784.]

Ben Ayed, N., and A. Oueslati (1988), Déformations tectoniques dans le Quaternaire récent de Ras Engela (région de Bizerte, Tunisie septentrionale), *Geol. Mediterr.*, *64*(2), 17–21, doi:10.3406/medit.1988.2543.

Ben Ayed, N., and F. Zargouni (1990), *Carte sismotectonique de la Tunisie à l'échelle 1/1000 000*, Fondation Nationale de la Recherche Scientifique, Tunisia.

Ben Ferjani, A., P. F. Burollet, and F. Mejri (1990), Petroleum geology of Tunisia, ETAP, Tunis.

Bernardi, F., J. Braunmiller, U. Kradolfer, and D. Giardini (2004), Automatic regional moment tensor inversion in the European-Mediterranean region, *Geophys. J. Int.*, *157*(2), 703–716.

Bianca, M., C. Monaco, L. Tortorici, and L. Cernobori (1999), Quaternary normal faulting in southeastern Sicily (Italy): A seismic source for the 1693 large earthquake, *Geophys. J. Int.*, *139*(2), 370–394.

Billi, A., C. Faccenna, O. Bellier, L. Minelli, G. Neri, C. Piromallo, D. Presti, D. Scrocca, and E. Serpelloni (2011), Recent tectonic reorganization of the Nubia-Eurasia convergent boundary heading for the closure of the western Mediterranean, *Bull. Soc. Geol. Fr.*, *182*(4), 279–303.

Bird, P. (2003), An updated digital model of plate boundaries, *Geochem. Geophys. Geosyst.*, *4*, 1027, doi:10.1029/2001GC000252.

Boccaletti, M., R. Nicolich, and L. Tortorici (1990), New data and hypothesis on the development of the Tyrrhenian basin, *Palaeogeogr. Palaeoclimatol. Palaeoecol.*, *77*(1), 15–40.

Bott, M. H. P. (1959), The mechanics of oblique slip faulting, *Geol. Mag.*, *96*(02), 109–117.

Bousquet, J. C., and H. Philip (1981), Les caractéristiques de la néotectonique en Méditerranée occidentale, in *Sedimentary Basins of the Mediterranean Murgins*, CNR, It. Proj. Oceanogr., Tecnoprint, pp. 389–405.

Bracène, R., and D. Frizon de Lamotte (2002), The origin of intraplate deformation in the Atlas system of western and central Algeria: From Jurassic rifting to Cenozoic–Quaternary inversion, *Tectonophysics*, *357*(1), 207–226.

Braunmiller, J., U. Kradolfer, M. Baer, and D. Giardini (2002), Regional moment tensor determination in the European–Mediterranean area—Initial results, *Tectonophysics*, *356*(1), 5–22.

Buforn, E., M. Bezzeghoud, A. Udias, and C. Pro (2004), Seismic sources on the Iberia-African plate boundary and their tectonic implications, *Pure Appl. Geophys.*, *161*(3), 623–646.

Buness, H., P. Giese, C. Bobier, C. Eva, F. Merlanti, R. Pedone, L. Jenatton, D. Nguyen, F. Thouvenot, and F. Egloff (1992), The EGT-85 seismic experiment in Tunisia: A reconnaissance of the deep structures, *Tectonophysics*, *207*(1–2), 245–267.

Burollet, P. (1991), Structures and tectonics of Tunisia, *Tectonophysics*, *195*(2), 359–369.

Campbell, D. L. (1978), Investigation of the stress-concentration mechanism for intraplate earthquakes, *Geophys. Res. Lett.*, *5*(6), 477–479, doi:10.1029/GL005i006p00477.

Carey, E., and B. Brunier (1974), Analyse théorique et numérique d'un modèle mécanique élémentaire appliqué à l'étude d'une population de failles, *CR Acad. Sci. Paris*, *279*, 891–894.

Carey-Gailhardis, E., and J. L. Mercier (1987), A numerical method for determining the state of stress using focal mechanisms of earthquake populations: Application to Tibetan teleseisms and microseismicity of southern Peru, *Earth Planet. Sci. Lett.*, *82*(1), 165–179.

Carminati, E., M. Wortel, W. Spakman, and R. Sabadini (1998), The role of slab detachment processes in the opening of the western–central Mediterranean basins: Some geological and geophysical evidence, *Earth Planet. Sci. Lett.*, *160*(3), 651–665.

Casero, P., and F. Roure (1994), Neogene deformations at the Sicilian–North African plate boundary, in *Peri-Tethyan Platforms*, pp. 27–50, Editions Technip, Paris.

Catalano, S., G. De Guidi, C. Monaco, G. Tortorici, and L. Tortorici (2008), Active faulting and seismicity along the Siculo–Calabrian Rift Zone [southern Italy], *Tectonophysics*, *453*(1), 177–192.

Catalano, S., G. De Guidi, G. Lanzafame, C. Monaco, and L. Tortorici (2009), Late Quaternary deformation on the island on Pantelleria: New constraints for the recent tectonic evolution of the Sicily Channel Rift [southern Italy], *J. Geodyn.*, *48*(2), 75–82.

Chiarabba, C., P. De Gori, and F. M. Mele (2015), Recent seismicity of Italy: Active tectonics of the central Mediterranean region and seismicity rate changes after the M_w 6.3 L'Aquila earthquake, *Tectonophysics*, *638*, 82–93.

Chihi, L. (1992), Seismotectonic study in central and southern Tunisia, *Tectonophysics*, *209*(1), 175–178.

Civello, S., and L. Margheriti (2004), Toroidal mantle flow around the Calabrian slab (Italy) from SKS splitting, *Geophys. Res. Lett.*, *31*, L10601, doi:10.1029/2004GL019607.

Civile, D., E. Lodolo, D. Accettella, R. Geletti, Z. Ben-Avraham, M. Deponte, L. Facchin, R. Ramella, and R. Romeo (2010), The Pantelleria graben (Sicily Channel, central Mediterranean): An example of intraplate "passive" rift, *Tectonophysics*, *490*(3), 173–183.

Coward, M. (1994), Inversion tectonics, in *Continental Deformation*, pp. 289–304, Pergamon Press, Oxford, U. K.

D'Agostino, N., E. D'Anastasio, A. Gervasi, I. Guerra, M. R. Nedimović, L. Seeber, and M. Steckler (2011), Forearc extension and slow rollback of the Calabrian Arc from GPS measurements, *Geophys. Res. Lett.*, *38*, L17304, doi:10.1029/2011GL048270.

Delvaux, D., and A. Barth (2010), African stress pattern from formal inversion of focal mechanism data, *Tectonophysics*, *482*(1), 105–128.

Delvaux, D., and B. Sperner (2003), New aspects of tectonic stress inversion with reference to the Tensor program, *Geol. Soc. London Spec. Publ.*, *212*(1), 75–100.
Delvaux, D., R. Moeys, G. Stapel, C. Petit, K. Levi, A. Miroshnichenko, V. Ruzhich, and V. San'kov (1997), Paleostress reconstructions and geodynamics of the Baikal region, central Asia, Part 2. Cenozoic rifting, *Tectonophysics*, *282*(1), 1–38.
DeMets, C., R. G. Gordon, D. Argus, and S. Stein (1990), Current plate motions, *Geophys. J. Int.*, *101*(2), 425–478.
De Voogd, B., C. Truffert, N. Chamot-Rooke, P. Huchon, S. Lallemant, and X. Le Pichon (1992), Two-ship deep seismic soundings in the basins of the Eastern Mediterranean Sea (Pasiphae cruise), *Geophys. J. Int.*, *109*(3), 536–552.
El Ghali, A., N. Ben Ayed, C. Bobier, F. Zargouni, and A. Krima (2003), Les manifestations tectoniques synsédimentaires associées à la compression éocène en Tunisie: Implications paléogéographiques et structurales sur la marge Nord-Africaine, *C. R. Geosci.*, *335*(9), 763–771.
Faccenna, C., C. Piromallo, A. Crespo-Blanc, L. Jolivet, and F. Rossetti (2004), Lateral slab deformation and the origin of the western Mediterranean arcs, *Tectonics*, *23*, TC1012, doi:10.1029/2002TC001488.
Faccenna, C., L. Civetta, M. D'Antonio, F. Funiciello, L. Margheriti, and C. Piromallo (2005), Constraints on mantle circulation around the deforming Calabrian slab, *Geophys. Res. Lett.*, *32*, L06311, doi:10.1029/2004GL021874.
Faccenna, C., F. Funiciello, L. Civetta, M. D'Antonio, M. Moroni, and C. Piromallo (2007), Slab disruption, mantle circulation, and the opening of the Tyrrhenian basins, *Geol. Soc. Am. Spec. Pap.*, *418*, 153–169.
Faccenna, C., T. W. Becker, L. Auer, A. Billi, L. Boschi, J. P. Brun, F. A. Capitanio, F. Funiciello, F. Horvàth, and L. Jolivet (2014), Mantle dynamics in the Mediterranean, *Rev. Geophys.*, *52*, 283–332, doi:10.1002/2013RG000444.
Frohlich, C. (1992), Triangle diagrams: Ternary graphs to display similarity and diversity of earthquake focal mechanisms, *Phys. Earth Planet. Inter.*, *75*, 193–198.
Gephart, J. W. (1990), FMSI: A FORTRAN program for inverting fault/slickenside and earthquake focal mechanism data to obtain the regional stress tensor, *C. R. Geosci.*, *16*(7), 953–989.
Gephart, J. W., and D. W. Forsyth (1984), An improved method for determining the regional stress tensor using earthquake focal mechanism data: Application to the San Fernando earthquake sequence, *J. Geophys. Res.*, *89*(B11), 9305–9320.
Gharbi, M., O. Bellier, A. Masrouhi, and N. Espurt (2014), Recent spatial and temporal changes in the stress regime along the southern Tunisian Atlas front and Gulf of Gabes: New insights from fault kinematics inversion, *Tectonophysics*, *626*, 120–136.
Giunta, G., D. Luzio, F. Agosta, M. Calò, F. Di Trapani, A. Giorgianni, E. Oliveri, S. Orioli, M. Perniciaro, and M. Vitale (2009), An integrated approach to investigate the seismotectonics of northern Sicily and southern Tyrrhenian, *Tectonophysics*, *476*(1), 13–21.
Göğüş, O. H., and R. N. Pysklywec (2008), Mantle lithosphere delamination driving plateau uplift and synconvergent extension in eastern Anatolia, *Geology*, *36*(9), 723–726.
Govers, R., and M. Wortel (2005), Lithosphere tearing at STEP faults: Response to edges of subduction zones, *Earth Planet. Sci. Lett.*, *236*(1), 505–523.
Grad, M., and T. Tiira (2009), The Moho depth map of the European Plate, *Geophys. J. Int.*, *176*(1), 279–292.
Grasso, M., C. D. Reuther, and L. Tortorici (1992), Neotectonic deformations in SE Sicily: The Ispica fault, evidence of late Miocene-Pleistocene decoupled wrenching within the central Mediterranean stress regime, *J. Geodyn.*, *16*(1), 135–146.
Gueddiche, M., H. Harjono, N. Ben Ayed, M. Hfaiedh, M. Diament, and J. Dubois (1992), Analyse de la séismicité et mise en évidence d'accidents actifs dans le nord de la Tunisie, *Bull. Soc. Geol. France.*, *163*(4), 415–425.
Gueddiche, M., N. Ben Ayed, G. Mohammadioun, B. Mohammadioun, A. El Ghali, H. Chekhma, M. Diament, and J. Dubois (1998), Etude sismotectonique de la Tunisie nord-orientale, *Bull. Soc. Geol. France.*, *169*(6), 789–796.
Guillaume, B., L. Husson, F. Funiciello, and C. Faccenna (2013), The dynamics of laterally variable subductions: Laboratory models applied to the Hellenides, *Solid Earth*, *4*, 179–200.
Harbi, A., S. Maouche, and A. Ayadi (1999), Neotectonics and associate seismicity in the eastern Tellian Atlas of Algeria, *J. Seismol.*, *3*(1), 95–104.
Heidbach, O., M. Tingay, A. Barth, J. Reinecker, D. Kurfeß, and B. Müller (2010), Global crustal stress pattern based on the World Stress Map database release 2008, *Tectonophysics*, *482*(1), 3–15.
Hfaiedh, M., N. Ben Ayed, and J. Dorel (1985), Etude néotectonique et sismotectonique de la Tunisie nord-orientale, *Note Serv. Géol. Tunisie*, *16*, 41–56.
Imanishi, K., N. Takeda, Y. Kuwahara, and N. Koizumi (2011), Enhanced detection capability of non-volcanic tremor using a 3-level vertical seismic array network, VA-net, in southwest Japan, *Geophys. Res. Lett.*, *38*, L20305, doi:10.1029/2011GL049071.
Jackson, J. (1987), Active normal faulting and crustal extension, *Geol. Soc. London Spec. Publ.*, *28*(1), 3–17.
Jallouli, C., and K. Mickus (2000), Regional gravity analysis of the crustal structure of Tunisia, *J. Afr. Earth Sci.*, *30*(1), 63–78.
Jolivet, L., and C. Faccenna (2000), Mediterranean extension and the Africa-Eurasia collision, *Tectonics*, *19*(6), 1095–1106, doi:10.1029/2000TC900018.
Jolivet, L., C. Faccenna, and C. Piromallo (2009), From mantle to crust: Stretching the Mediterranean, *Earth Planet. Sci. Lett.*, *285*(1), 198–209.
Kamoun, Y., D. Sorel, C. Viguier, and N. B. Ayed (1980), Un grand accident subméridien d'âge post-Tyrrhénien en Tunisie orientale: le décrochement sénestre de Skanès (Monastir)-Hammamet, *CR. Acad. Sci. Paris Série D*, *290*, 647–649.
Lavecchia, G., F. Ferrarini, R. de Nardis, F. Visini, and M. S. Barbano (2007), Active thrusting as a possible seismogenic source in Sicily (southern Italy): Some insights from integrated structural–kinematic and seismological data, *Tectonophysics*, *445*(3), 145–167.
Le Pichon, X., F. Bergerat, and M. J. Roulet (1988), Plate kinematics and tectonics leading to the Alpine belt formation; A new analysis, *Geol. Soc. Am. Spec. Pap.*, *218*, 111–132.
Lucente, F. P., L. Margheriti, C. Piromallo, and G. Barruol (2008), Seismic anisotropy reveals the long route of the slab through the western-central Mediterranean mantle, *Earth Planet. Sci. Lett.*, *241*(3), 517–529.
Lund, B., and J. Townend (2007), Calculating horizontal stress orientations with full or partial knowledge of the tectonic stress tensor, *Geophys. J. Int.*, *170*(3), 1328–1335.
Macchiavelli, C., S. Mazzoli, A. Megna, F. Saggese, S. Santini, and S. Vitale (2012), Applying the Multiple Inverse Method to the analysis of earthquake focal mechanism data: New insights into the active stress field of Italy and surrounding regions, *Tectonophysics*, *580*, 124–149.
Mastrolembo Ventura, B., E. Serpelloni, A. Argnani, A. Bonforte, R. Bürgmann, M. Anzidei, P. Baldi, and G. Puglisi (2014), Fast geodetic strain-rates in eastern Sicily (southern Italy): New insights into block tectonics and seismic potential in the area of the great 1693 earthquake, *Earth Planet. Sci. Lett.*, *404*(0), 77–88.
Maury, R. C., S. Fourcade, C. Coulon, H. Bellon, A. Coutelle, A. Ouabadi, B. Semroud, M. h. Megartsi, J. Cotten, and O. Belanteur (2000), Post-collisional Neogene magmatism of the Mediterranean Maghreb margin: A consequence of slab breakoff, C. R. Acad. Sci., Ser. IIa: *Earth Planet. Sci.*, *331*(3), 159–173.
McClusky, S., R. Reilinger, S. Mahmoud, D. B. Sari, and A. Tealeb (2003), GPS constraints on Africa (Nubia) and Arabia plate motions, *Geophys. J. Int.*, *155*(1), 126–138.

Meghraoui, M., and S. Pondrelli (2012), Active faulting and transpression tectonics along the plate boundary in North Africa, *Ann. Geophys.*, *55*, 5, doi:10.4401/ag-4970.
Mejri, L. (2012), Tectonique quaternaire, paléosismicité et sources sismogéniques en Tunisie nord-orientale: étude de la faille d'Utique Thèse Doc. Univ. Toulouse, pp. 184.
Mezcua, J., and J. Martınez Solares (1983), Seismicity of the Ibero–Maghrebian area Instituto Geográfico Nacional Report, Madrid.
Michael, A. J. (1987), Use of focal mechanisms to determine stress: A control study, *J. Geophys. Res.*, *92*(B1), 357–368, doi:10.1029/JB092iB01p00357.
Montone, P., M. T. Mariucci, S. Pondrelli, and A. Amato (2004), An improved stress map for Italy and surrounding regions (central Mediterranean), *J. Geophys. Res.*, *109*, B10410, doi:10.1029/2003JB002703.
Morel, J. L., and M. Meghraoui (1996), Goringe-Alboran-Tell tectonic zone: A transpression system along the Africa-Eurasia plate boundary, *Geology*, *24*(8), 755–758.
Negredo, A. M., R. Sabadini, G. Bianco, and M. Fernandez (1999), Three-dimensional modelling of crustal motions caused by subduction and continental convergence in the central Mediterranean, *Geophys. J. Int.*, *136*(1), 261–274.
Neri, M., F. Casu, V. Acocella, G. Solaro, S. Pepe, P. Berardino, E. Sansosti, T. Caltabiano, P. Lundgren, and R. Lanari (2009), Deformation and eruptions at Mt. Etna (Italy): A lesson from 15 years of observations, *Geophys. Res. Lett.*, *36*, L02309, doi:10.1029/2008GL036151.
Nigro, F. (1998), Neotectonic events and kinematics of rhegmatic-like basins in Sicily and adjacent areas. Implications for a structural model of the Tyrrhenian opening, *Ann. Soc. Geol. Pol.*, *68*, 1–21.
Nocquet, J. M. (2012), Present-day kinematics of the Mediterranean: A comprehensive overview of GPS results, *Tectonophysics*, *579*, 220–242.
Nocquet, J.-M., and E. Calais (2004), Geodetic measurements of crustal deformation in the western Mediterranean and Europe, *Pure Appl. Geophys.*, *161*(3), 661–681.
Orioli, S., G. Giunta, A. Giorgianni, F. Di Trapani, and D. Luzio (2009), Relationships between seismicity and tectonic in northern Sicily and southern Tyrrhenian: Some important open problems, paper presented at EGU General Assembly Conference Abstracts.
Ousadou, F., L. Dorbath, A. Ayadi, C. Dorbath, and S. Gharbi (2014), Stress field variations along the Maghreb region derived from inversion of major seismic crisis fault plane solutions, *Tectonophysics*, *632*, 261–280.
Palano, M., L. Ferranti, C. Monaco, M. Mattia, M. Aloisi, V. Bruno, F. Cannavó, and G. Siligato (2012), GPS velocity and strain fields in Sicily and southern Calabria, Italy: Updated geodetic constraints on tectonic block interaction in the central Mediterranean, *J. Geophys. Res.*, *117* B07401, doi:10.1029/2012JB009254.
Petricca, P., M. M. Carafa, S. Barba, and E. Carminati (2013), Local, regional, and plate scale sources for the stress field in the Adriatic and Periadriatic region, *Mar. Pet. Geol.*, *42*, 160–181.
Philip, H. (1987), Plio-Quaternary evolution of the stress field in Mediterranean zones of subduction and collision, *Ann. Geophys.*, *5*, 301–320.
Philip, H., J. Andrieux, M. Dlala, L. Chihi, and N. B. Ayed (1986), Evolution tectonique mio-quaternaire du fosse de Kasserine (Tunisie centrale); Implications sur l'evolution geodynamique recente de la Tunisie, *Bull. Soc. Geol. Fr.*, *2*(4), 559–568.
Pierdominici, S., and O. Heidbach (2012), Stress field of Italy—Mean stress orientation at different depths and wave-length of the stress pattern, *Tectonophysics*, *532*, 301–311.
Piromallo, C., and A. Morelli (2003), *P* wave tomography of the mantle under the Alpine Mediterranean area, *J. Geophys. Res.*, *108*(B2), 2065, doi:10.1029/2002JB001757.
Pondrelli, S., S. Salimbeni, G. Ekström, A. Morelli, P. Gasperini, and G. Vannucci (2006), The Italian CMT dataset from 1977 to the present, *Phys. Earth Planet. Inter.*, *159*(3), 286–303.
Ragg, S., M. Grasso, and B. Müller (1999), Patterns of tectonic stress in Sicily from borehole breakout observations and finite element modeling, *Tectonics*, *18*(4), 669–685, doi:10.1029/1999TC900010.
Rebaï, S., H. Philip, and A. Taboada (1992), Modern tectonic stress field in the Mediterranean region: Evidence for variation in stress directions at different scales, *Geophys. J. Int.*, *110*(1), 106–140.
Reches, Z. E., G. Baer, and Y. Hatzor (1992), Constraints on the strength of the upper crust from stress inversion of fault slip data, *J. Geophys. Res.*, *97*(B9), 12,481–12,493, doi:10.1029/90JB02258.
Richert, J. (1971), Mise en évidence de quatre phases tectoniques successives en Tunisie, *Notes Serv. Géol. Tunisie*, *34*, 115–125.
Rouvier, H. (1977), Géologie de l'extreme Nord Tunisien: Tectoniques et Paléogéographies superposées à l'extrémité Nord-orientale de la chaine maghrébine Thèse d' Etat, Université Paris-VI, pp. 898 .
Saïd, A., D. Chardon, P. Baby, and J. Ouali (2011), Active oblique ramp faulting in the southern Tunisian Atlas, *Tectonophysics*, *499*(1), 178–189.
Schäfer, K. (1980), In situ strain measurements in Libya, in *Tectonic Stresses in the Alpine-Mediterranean Region*, pp. 49–61, Springer, Vienna.
Sébrier, M., L. Siame, E. M. Zouine, T. Winter, Y. Missenard, and P. Leturmy (2006), Active tectonics in the Moroccan High Atlas, *C. R. Geosci.*, *338*(1), 65–79.
Sella, G. F., T. H. Dixon, and A. Mao (2002), REVEL: A model for recent plate velocities from space geodesy, *J. Geophys. Res.*, *107*(B4), 2081, doi:10.1029/2000JB000033.
Serpelloni, E., G. Vannucci, S. Pondrelli, A. Argnani, G. Casula, M. Anzidei, P. Baldi, and P. Gasperini (2007), Kinematics of the western Africa-Eurasia plate boundary from focal mechanisms and GPS data, *Geophys. J. Int.*, *169*(3), 1180–1200.
Serpelloni, E., C. Faccenna, G. Spada, D. Dong, and S. D. Williams (2013), Vertical GPS ground motion rates in the Euro-Mediterranean region: New evidence of velocity gradients at different spatial scales along the Nubia-Eurasia plate boundary, *J. Geophys. Res. Solid Earth*, *118*, 6003–6024, doi:10.1002/2013JB010102.
Singer, J., T. Diehl, S. Husen, E. Kissling, and T. Duretz (2014), Alpine lithosphere slab rollback causing lower crustal seismicity in northern foreland, *Earth Planet. Sci. Lett.*, *397*, 42–56.
Sorel, D., Y. Kamoun, M. Sayadi, C. Viguier, and N. Ben Ayed (1983), Décrochement d'âge historique et risque sismique dans la région de Monastir (Tunisie orientale), *Note Serv Géol Tunisie*, *47*, 35–41.
Swezey, C. (1996), Structural controls on Quaternary depocentres within the Chotts Trough region of southern Tunisia, *J. Afr. Earth Sci.*, *22*(3), 335–347.
Valensise, G., and D. Pantosti (1992), A 125 kyr-long geological record of seismic source repeatability: The Messina Straits (southern Italy) and the 1908 earthquake (M_s 71/2), *Terra Nova*, *4*(4), 472–483.
Vannucci, G., and P. Gasperini (2004), The new release of the database of Earthquake Mechanisms of the Mediterranean Area (EMMA version 2), *Ann. Geophys.*, *47*(Suppl. 1), 307–334.
Vially, R., J. Letouzey, F. Benard, N. Haddadi, G. Desforges, H. Askri, and A. Boudjema (1994), Basin inversion along the North African Margin. The Saharan Atlas (Algeria), in *Peri-tethyan Platforms*, pp. 79–118, Technip, Paris.
Winnock, E., and F. Bea (1979), Structure de la mer Pélagienne, *Géol. Méditerr.*, *4*, 35–40.
Wortel, M., and W. Spakman (2000), Subduction and slab detachment in the Mediterranean-Carpathian region, *Science*, *290*(5498), 1910–1917.

Wortel, R., R. Govers, and W. Spakman (2009), Continental collision and the STEP-wise evolution of convergent plate boundaries: From structure to dynamics, in *Subduction Zone Geodynamics*, pp. 47–59, Springer, Berlin Heidelberg.

Wuestefeld, A., G. H. R. Bokelmann, G. Barruol, and J. P. Montagner, (2009), Identifying global seismic anisotropy patterns by correlating shear wave splitting and surface-wave data, *Phys. Earth Planet. Int.*, *176*, 198–212.

Zargouni, F., and M. Ruhland (1981), Style de déformation du Quaternaire récent lié au coulissement de la faille de Gafsa et chronologie des phases tectoniques de l'Atlas méridional tunisien, *CR Acad. Sci. Paris*, *292*, 912–915.

Zhong, S., M. T. Zuber, L. Moresi, and M. Gurnis (2000), Role of temperature dependent viscosity and surface plates in spherical shell models of mantle convection, *J. Geophys. Res.*, *105*(B5), 11,063–11,082, doi:10.1029/2000JB900003.

Zoback, M. L. (1992), First and second order patterns of stress in the lithosphere: The World Stress Map project, *J. Geophys. Res.*, *97*(B8), 11,703–11,728, doi:10.1029/92JB00132.

Zouaghi, T., M. Bédir, and M. H. Inoubli (2005), 2D seismic interpretation of strike-slip faulting, salt tectonics, and Cretaceous unconformities, Atlas Mountains, central Tunisia, *J. Afr. Earth Sci.*, *43*(4), 464–486.